THE UNIVERSITY OF OKLAHOMA

GRADUATE COLLEGE

STUDY OF FLUX-TRAPPING IN SUPERCONDUCTING TIN-INDIUM

A DISSERTATION

SUBMITTED TO THE GRADUATE FACULTY

in partial fulfillment of the requirements for the

degree of

DOCTOR OF PHILOSOPHY

BY

Manjula Damji Ghalla

Norman, Oklahoma

1971

STUDY OF FLUX-TRAPPING IN SUPERCONDUCTING TIN-INDIUM

APPROVED BY

E. R. Hansen

Gene B. Parker

R. Craig Varner

Raymond D. Daniels

DISSERTATION COMMITTEE

ABSTRACT

The reduced surface resistance r of superconducting lead at 12 GHz is determined from measurements of the Q of high-Q superconducting lead plated cavity resonant in the TE_{011} mode. Q's as high as 196.5×10^6 were obtained. The results are compared to r_{AGK}, the theoretical surface resistance derived by Abrikosov, Gor'kov and Khalatnikov. It is found that $r = 7.326\ r_{AGK} + 0.0002826$ using the value of $1.97\ k_B T_c$ for the energy gap parameter at $0^\circ K$. Also, r obeys the Pippard temperature dependence, P(t), with $r = 0.0971\ P(t) - 0.0001795$.

The cavity is used to study the flux-trapping in Sn-In with one of its end plates replaced by a sample of Sn-In. In the presence of flux-trapping, the surface resistance of 4% and 5% In-Sn (annealed for 24 hours at $200^\circ C$) follows the Pippard temperature dependence. By applying the magnetic field both before and after the lead cavity walls become superconducting, it is possible to estimate A_o, the area that traps flux in the Sn-In sample at its transition into the superconducting state. The residual losses due to flux-

trapping are found to be proportional to the applied magnetic field. Flux-trapping in these samples is found to be structure sensitive rather than impurity sensitive.

Measurements on a laboratory-made 13% In-Sn sample confirmed the structure sensitivity of flux-trapping in a lightly annealed sample. Measurements were also made on a laboratory made 3% In-Sn alloy as a function of annealing time, starting with the cold-rolled alloy. The Pippard temperature dependence is observed. For a cold-rolled sample, the low critical field regions which trap flux are shown to decrease in area exponentially with the constant temperature annealing time.

ACKNOWLWDGEMENTS

My sincere thanks are due to Dr. Clovis Roland Haden for suggesting the research problem. His constant guidance and encouragement during the course of the experiments and the writing of this dissertation are most appreciated.

Helpful suggestions from Dr. H. J. Halama of the Brookhaven National Laboratory regarding the electroplating process are gratefully acknowledged. Thanks are also due to "Woody" for the fine machine work he cheerfully did and to "Charlie" for keeping me well supplied with 200 proof alcohol.

Finally, thanks are extended to the United States Atomic Energy Commission for funding this research.

TABLE OF CONTENTS

LIST OF ILLUSTRATIONS

LIST OF ILLUSTRATIONS--Continued

STUDY OF FLUX-TRAPPING IN SUPERCONDUCTING TIN-INDIUM

CHAPTER I

INTRODUCTION

A superconductor exhibits two fundamental characteristics: 1) the absence of d.c. resistance and 2) the expulsion of magnetic flux. When a superconductor is cooled in the absence of a magnetic field, its d.c. resistance drops abruptly to zero at the critical temperature T_c. Below the critical temperature, an applied magnetic field above a critical value can cause the resistance to reappear.

An external magnetic field below the critical value is expelled almost completely from a superconducting specimen. The interior of the sample is shielded from magnetic flux by surface currents which penetrate below the surface to a characteristic depth called the penetration depth, λ. The applied magnetic field penetrates a thin surface region and decays exponentially from its value at the surface with this characteristic length. For a type I superconductor of zero demagnetization constant, the critical magnetic field for

flux penetration is the same as for the return of normal resistance. The field at which the transition occurs is called the bulk critical field, H_c, and its approximate temperature dependence is given by[35]

$$H_c = H_o(1-t^2) \qquad (1.1)$$

where H_o = critical field at 0^oK

and $t = T/T_c$ is the reduced temperature.

When a type I superconducting specimen of non-zero demagnetization constant is placed in an applied magnetic field of increasing strength the magnetic field distribution at the surface of the specimen is non-uniform. When the field reaches its critical value over part of the surface, the entire specimen is subdivided into alternating normal and superconducting regions. The specimen is said to be in an intermediate state. The interior of a normal region has $H = H_c$ while the interior of a superconducting region has $H = 0$. As the applied magnetic field is increased, the normal regions grow in size and the superconducting regions shrink until the applied magnetic field reaches H_c, when the penetration is complete.

When a type II superconducting specimen of zero demagnetization constant is placed in an increasing magnetic field, the flux penetration begins at a field H_{c1}, which is lower than the field H_{c2} at which the normal resistance reappears. As the field is increased from H_{c1} to H_{c2}, more and more flux

penetrates until, at H_{c2}, the bulk of the specimen becomes normal. Between H_{c1} and H_{c2} the specimen is said to be in a mixed state.

The flux that exists inside the bulk of a superconducting body when it is either in the mixed state or in the intermediate state is completely removed when the external magnetic field is removed, that is, the magnetization curve is reversible for the mixed and intermediate states. However, when a multiply connected superconductor is cooled in the presence of a magnetic field, the flux threading the hollow regions of the superconductor cannot be dispersed by removing the external field because of the persistent currents induced in the superconductor. A simply connected non-homogeneous superconductor can also trap flux. Structural imperfections and impurities can create within the superconductor multiply connected regions with anomalously high critical fields. When such a non-ideal superconducting specimen is made entirely normal in an external magnetic field and the field is then decreased continuously, the high critical field regions are the first to become superconducting. The flux threading these multiply connected superconducting regions at the moment of their transition into the superconducting state will no longer be able to escape when the external magnetic field is reduced to zero. Thus, such an imperfect superconductor traps flux when it is made superconducting in the presence of an external magnetic field, and it retains a paramagnetic moment when the

field is removed. The magnetization curve for a type I non-homogeneous superconductor in the form of a long cylinder parallel to the applied magnetic field is shown in Figure 1.1 where M is the magnetization and H_e is the applied field. The ratio of m to $-H_c$ is called the fraction of trapped flux. Hysteresis effects at d.c. have long been reported[1-5] both for type I as well as type II superconductors.

Pippard[7] and Doidge[8] have studied flux-trapping in thin rods of single crystal Sn-In, with indium concentration varying from 0 to 3.5% by weight. They found the amount of flux trapped to depend on various types of imperfections in the specimens, namely, surface roughness, polycrystallinity and inhomogeneity of impurity. Other experimenters[9-11] have found that the amount of trapped flux depends upon the rate at which the magnetic field is turned off and the relative direction of the specimen and the field.

The extreme structure and impurity sensitivity of flux-trapping in superconductors has stimulated a growing interest for an improved understanding of the nature of flux-trapping centers in superconductors. Much of this interest has arisen since Kunzler's[24] discovery of the possibility of using superconductors to generate high magnetic fields. The high current carrying capability of niobium alloys is believed[30] to be due to the presence of inhomogeneities or defects in the material, such as dislocations, which can trap flux.

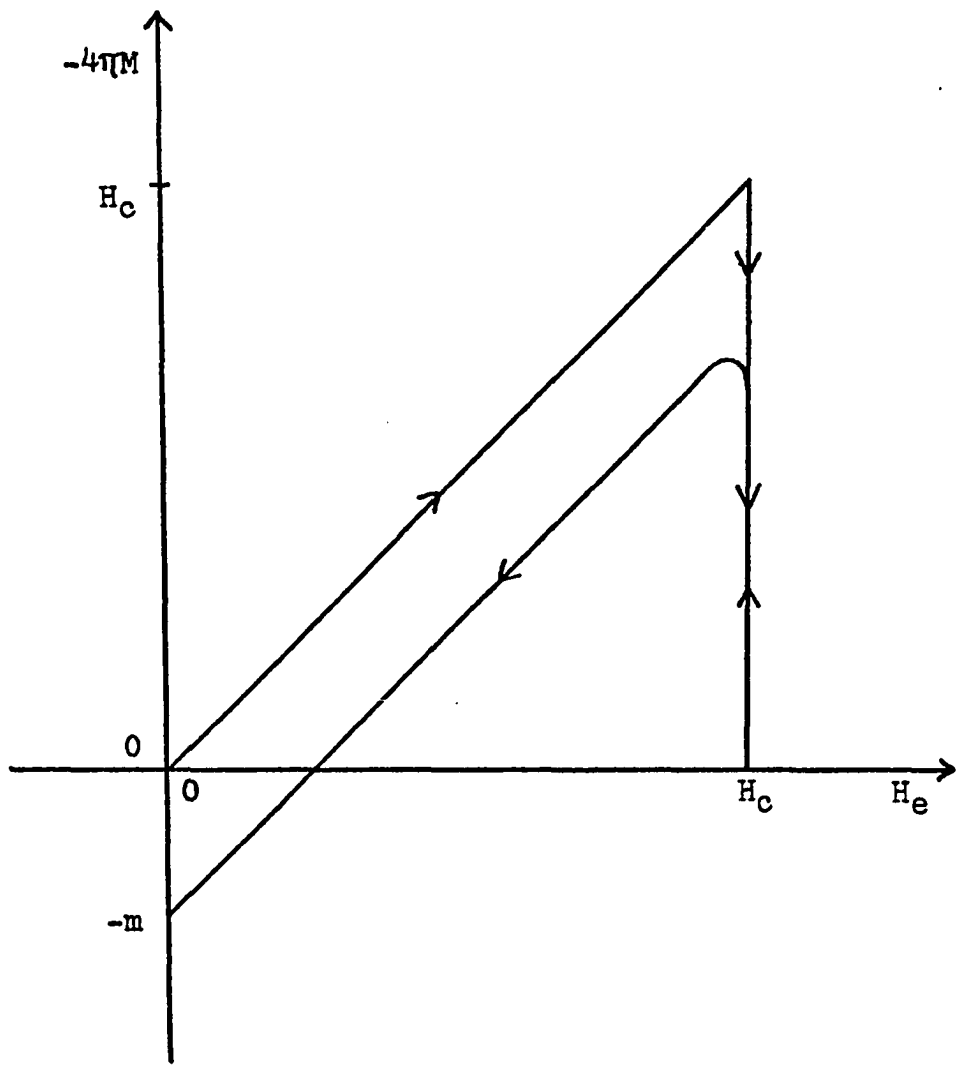

Figure 1.1

Magnetization curve for a non-homogeneous type I superconductor of zero demagnetization constant

Although the d.c. resistance of a superconductor drops abruptly to zero at the transition, the a.c. resistance even at frequencies well below ν_g is finite at all finite temperatures. Here ν_g is the gap frequency given by equation 1.2 below. Above ν_g the a.c. resistance of a superconducting specimen is the same as if the specimen were normal.

$$h\nu_g = 2\epsilon(0) \qquad (1.2)$$

where $2\epsilon(0)$ is the energy gap between the superconducting and the normal states.

According to the two fluid theory of Görter and Casimir, the conduction electron fluid in the superconducting state can be divided into a normal component and a super component. Whereas the electrons in the normal component interact with the atomic lattice and behave like conduction electrons in non-superconducting specimens, the motion of superelectrons is resistanceless. If n_n and n_s are the densities of the electrons in the normal and super components, respectively, then Görter and Casimir have postulated that

$$n_n = nt^4 \quad \text{and} \quad n_s = n(1-t^4) \qquad (1.3)$$

where $n = n_n + n_s$ is the density of the total number of electrons. As seen from equation 1.3, between the transition temperature and $0^\circ K$, the fraction of electrons in the superconducting state increases steadily from 0 to 1. Below the transition temperature the d.c. resistance disappears since the super electrons, however few, can carry a lossless current and short circuit the normal electrons. However, an electric field is

required to sustain an alternating current in a superconducting specimen because of the inertia of the super electrons. As first pointed out by H. London, this electric field, while acclerating the super electrons, also acts on the normal electrons and gives rise to dissipation of power. Thus, according to the two fluid theory, the decrease in the a.c. resistance at the transition temperature is gradual; the a.c. resistance is finite at all finite temperatures and it should reach zero at $0^{o}K$.

The first high frequency surface impedance measurements were reported by London[12]. Since then, there have been many investigations on several metals and there is now a sizable amount of empirical data on the subject. The theoretical analysis of the phenomenon has proceeded in parallel with experiment, starting first with fairly simple phenomenological models and leading most recently to descriptions based on the microscopic BCS theory.

The theoretical surface resistance of isotropic weak coupling superconductors at microwave frequencies was derived by Mattis and Bardeen[14] and, independently by Abrikosov, Gor'kov and Khalatnikov (AGK)[29]. Analytical expressions for the reduced surface resistance, which is the ratio of the superconducting to normal surface resistance, under zero d.c. magnetic field were derived by AGK in the Pippard limit which is characterized by an infinite mean free path, $\ell = \infty$, and a

corresponding coherence distance ξ_o. For $\hbar\omega \ll k_BT \ll \Delta$, they obtained the approximate relation

$$r_{AGK} = \frac{8}{3\pi}\left(\frac{\hbar\omega}{\pi\Delta}\right)^{1/3} \sinh\left(\frac{\hbar\omega}{2k_BT}\right) K_o\left(\frac{\hbar\omega}{2k_BT}\right) \exp\left(-\frac{\Delta}{k_BT}\right) \qquad (1.4)$$

where $\hbar$ is the normalized Planck constant,

ω is the a.c. frequency in radians/sec,

k_B is the Boltzmann constant,

Δ is the energy gap parameter

and K_o is the modified Bessel function of 0 order.

The temperature dependence of the gap may be approximated[25] by

$$\Delta = \Delta(0) \cos(\tfrac{1}{2}\pi t^2) \qquad (1.5)$$

The theoretical behavior of superconductors in electromagnetic fields applies only to ideal metals. The real situation differs from theory at lower temperatures because of the residual reduced surface resistance, r_o, which is due to various loss mechanisms and is not an intrinsic property of the superconductor. Contributions to r_o stem, for example, from losses in the external circuitry or losses caused by flux-trapping, but other possible origins have been suggested[20,26,27]. When the residual losses are independent of temperature or only weakly dependent on temperature, the reduced surface resistance may be written as[31]

$$r = A\, r_{AGK} + r_o \qquad (1.6)$$

where A and r_o are both independent of temperature. The temperature dependence of this equation was experimentally

verified for pure lead at 12 GHz and is further discussed in Chapter 4.

Pippard has derived the following semi-empirical relation for the reduced surface resistance[35].

$$r = A(\nu)\ P(t) + r_o \qquad (1.7)$$

where $A(\nu)$ is a function of frequency but is independent of temperature,

and $P(t) = t^4\ (1-t^2)\ /\ (1-t^4)^2$

This equation was compared with the experimental reduced surface resistance of pure lead at 12 GHz. In investigations of surface resistance it has been customary[28] to plot the observed reduced surface resistance against P(t) and by linear extrapolation determine the residual term r_o. However, the observed residual losses are not temperature independent in general unless extreme precautions are taken.

Haden[20] has proposed a hysteresis loss model for the observed temperature dependent residual loss in superconductors. He arrives at equation 1.8 for the power loss due to the trapping of the r.f. magnetic field.

$$P_r = 4\ K\ H_{cl}\ \nu\ N\ \lambda\ (H_{mo} - H_{cl}(1 + \ln(H_{mo}/H_{cl}))) \qquad (1.8)$$

where K is a constant,

ν is the frequency,

H_{cl} is the low effective critical field surrounding a non-superconducting channel,

H_{mo} is the magnetic field at the surface

and λ is the penetration depth.

Haden has experimentally verified the observed surface resistance to be a linear superposition of flux-trapping and ordinary surface resistances. He has also verified the temperature, frequency and other dependences predicted by his model.

Pierce et al[16] have proposed another model for the temperature dependent residual loss when the superconductor is cooled in the presence of a d.c. magnetic field. Their model applies in the skin depth limit when $\lambda >> \delta$, where δ is the classical skin depth. They assume that the flux is trapped in regions whose size is determined by the requirement that the field in the normal regions be equal to the critical field. The additional loss associated with the trapped flux is then proportional to the normal area which is inversely proportional to the critical field. They have proposed that the observed surface resistance can be fitted reasonably well by adding to the ordinary surface resistance a term proportional to $(1-t^2)^{-1}$.

Victor[21] has modified the above model of Pierce et al for the penetration depth limit when $\lambda << \delta$. He has shown that it is necessary to add a term of the form $r_h(0)V(t)$ to the right hand side of equation 1.7, giving rise to

$$r = A(\nu)P(t) + r_h(0)V(t) + r_o \qquad (1.9)$$

where $r_h(0)$ is the value of the additional term at 0^oK and $V(t)$ is a function of temperature.

Victor has proposed that for $\lambda \ll \delta$, V(t), the temperature dependence of the trapped flux component of r is the product of the temperature dependences of the area that traps flux and the penetration depth of the r.f. currents.

When a foil of superconductor becomes superconducting in an applied magnetic field H_e, the amount of flux trapped is $H_e A_o$, where A_o is the area of low effective critical field at the moment of transition. As the temperature of the specimen is lowered the critical field increases as shown by equation 1.1. Since the field in the region that traps flux must always be equal to the critical field, the region that traps flux must shrink as the temperature is lowered such that the trapped flux, ϕ, is a constant. Therefore,

$$\phi = H_e A_o = H_o(1-t^2)\, A(t) \qquad (1.10)$$

where A(t) is the temperature dependent area that carries trapped flux. From equation 1.10,

$$A(t) = H_e A_o / (H_o(1-t^2)) \qquad (1.11)$$

The penetration depth has a temperature dependence[35] of the form $(1-t^4)^{-\frac{1}{2}}$. Therefore, the normal volume responsible for the residual surface resistance due to trapped flux is proportional to $H_e A_o/(H_o(1-t^2)(1-t^4)^{\frac{1}{2}})$. Since the normal surface resistance is constant over the temperature and magnetic field range of interest,

$$r_h(0)V(t) = k\, \frac{H_e A_o}{H_o(1-t^2)(1-t^4)^{\frac{1}{2}}} \qquad (1.12)$$

where k is a constant of proportionality

$$\text{and } V(t) = \frac{1}{(1-t^2)(1-t^4)^{\frac{1}{2}}} \qquad (1.13)$$

This is the essence of Victor's model, and he has verified the temperature and magnetic field dependences in the frequency range of 60 MHz to 340 MHz for pure tin. Victor's flux trapping model, which combines the best features of the other models described above, was applied to the experimental data reported in this dissertation.

The purpose of the research reported in this dissertation was to study the nature of flux trapping centers in superconductors. This study was made by observing the effect of annealing and impurity concentration on the residual reduced surface resistance due to trapped flux of delta phase tin-indium at a frequency of 12 GHz.

The primary quantity measured is τ, the time constant of decay of energy from a cavity resonator, one surface of which is the alloy specimen under study. The remaining surfaces of the cavity are lead plated and have negligible losses in comparison with the alloy specimens under study, as verified by the experimental data. The method of measuring τ and its relation to flux trapping is discussed in detail in Chapter II. Chapter III describes the laboratory procedures and Chapter IV contains the results and conclusions of the research.

CHAPTER II

THEORY OF MEASUREMENT

Method of Analysis

As mentioned in Chapter I, when a superconductor is cooled in the presence of a magnetic field, it can trap flux if it has multiply connected regions of high effective critical field. From equations 1.9, 1.12 and 1.13, it follows that at a constant frequency, the reduced surface resistance, r, of a superconductor with trapped flux is given by

$$r = \frac{R_s}{R_n} = A(\nu)P(t) + k\frac{H_e A_o}{H_o}V(t) + r_o \qquad (2.1)$$

where R_s is the superconducting surface resistance

and R_n is the normal surface resistance.

Over the temperature range of interest, Victor[21] has shown V(t) to be linearly related to P(t). In equation 2.1, V(t) can be approximated by

$$V(t) = 5.97\ P(t) + 1 \qquad (2.2)$$

Substituting for V(t) from equation 2.2 in equation 2.1 gives

$$R_s = \left(A(\nu) + k\frac{H_eA_o}{H_o}5.97\right)P(t)R_n + k\frac{H_eA_o}{H_o}R_n + r_oR_n \qquad (2.3)$$

Since R_n remains constant over the temperature and magnetic field range of interest, R_s is linearly related to P(t) and can be expressed as

$$R_s = m'P(t) + c' \qquad (2.4)$$

$$\text{where } m' = \left(A(\nu) + k\frac{H_eA_o}{H_o}5.97\right)R_n \qquad (2.5a)$$

$$\text{and } c' = \left(k\frac{H_eA_o}{H_o} + r_o\right)R_n \qquad (2.5b)$$

Now m' and c' can be found by plotting R_s versus P(t) with H_e as the parameter. Then, dm'/dH_e and dc'/dH_e can be found by plotting m' and c' versus H_e. From equations 2.5, both dm'/dH_e and dc'/dH_e are proportional to A_o. In superconductors, the flux is trapped at regions of low effective critical field, which are believed to be created by impurities and defects in the material. Therefore A_o, the area that traps flux at the moment of transition from the normal to the superconducting state must change with impurity content and/or annealing of the sample. This change in A_o can be observed by plotting dm'/dH_e and dc'/dH_e as functions of impurity concentration and annealing time.

The purpose of this research is to identify the nature of flux trapping sites in superconductors by correlating the variation of dm'/dH_e and dc'/dH_e with change in defect and impurity concentration of delta phase tin-indium. Since the

critical temperature of indium is lower than that of tin, the indium atoms serve as impurity centers in tin.

Flux trapping due to defects can be investigated by correlating the variation of dm'/dH_e and dc'/dH_e with the annealing time of the sample. When a cold-rolled material is annealed, energy is supplied to the atoms or molecules of the material, allowing them to escape the action of local stress fields[33]. The atoms and molecules diffuse throughout the material tending to make the irregular structure of the cold-rolled material more homogeneous. The amount of annealing is ideally exponential with time, the time constant itself being an exponential function of temperature[34].

$$D = D_o e^{-t/n} \tag{2.6}$$

$$n = n_o e^{-W/k_B T} \tag{2.7}$$

where D is a measure of the deformity,

n is the time constant,

and W is the activation energy.

Thus, the experimental problem is that of measuring the surface resistance of superconducting tin-indium foils as a function of temperature under different magnetic fields and for various impurity concentrations and annealing times.

Theory of Measurement of R_s

At microwave frequencies, the effective surface resistance R_s of a superconductor can be conveniently determined

from the unloaded quality factor Q_o of a resonant cavity whose walls are made of the superconductor under study. R_s and Q_o are related by the simple equation given by

$$R_s = G_o Z_o / Q_o \qquad (2.8)$$

where G_o is a geometrical factor

and Z_o is the characteristic impedance of free space in MKS units.

The Q of a cavity is defined as the ratio of the energy stored in the cavity to the energy lost per cycle. Several mechanisms can contribute to the energy loss in the cavity. These are:

1. The effective surface resistance loss in the cavity walls (cf. equation 2.3)
2. The surface dielectric loss in any film, such as an oxide film, that might form on the cavity wall; and the volume dielectric loss in the medium filling the cavity.
3. The losses due to currents crossing mechanical joints of the cavity.
4. Radiation losses through the iris which allows the flow of energy between the cavity and the external circuitry.
5. Losses in the energy coupling mechanism.

If Q_o, Q_d, Q_m, Q_r and Q_c are respectively the quality factors of the resonant cavity defined individually for each of the energy losses described in 1, 2, 3, 4 and 5 above,

then

$$\frac{1}{Q_\ell} = \frac{1}{Q_o} + \frac{1}{Q_d} + \frac{1}{Q_m} + \frac{1}{Q_r} + \frac{1}{Q_c} \tag{2.9}$$

where Q_ℓ is the loaded Q of the cavity.

Since the parameter of interest is the effective surface resistance of the cavity wall and Q_ℓ is the measured Q, we must have

$$Q_\ell \approx Q_o \tag{2.10}$$

Hence the energy losses described in 2, 3, 4 and 5 above must be minimized such that the condition given by the inequality 2.11 is satisfied.

$$\frac{1}{Q_d} + \frac{1}{Q_m} + \frac{1}{Q_r} + \frac{1}{Q_c} \ll \frac{1}{Q_o} \tag{2.11}$$

Methods of minimizing these losses and of measuring Q_o are described in detail in Chapter III. Once these are minimized, it is possible to analyze Q_o, or the effective surface resistance, breaking it down into the true surface resistance and the residual loss resistance.

CHAPTER III

EXPERIMENTAL WORK

Introduction

The most difficult part of the experimental work was that of satisfying the inequality 2.11 for the lead plated cavity. Once this was achieved, the surface resistance of tin-indium could be determined by measuring the Q of the lead plated cavity, whose one end plate was replaced by the tin-indium sample. Over the temperature range of interest the losses in the alloy are known to be much larger than the losses in the lead. The Q measured with the alloy specimen therefore corresponds to the losses in the alloy.

Lead Plating

In order to minimize the surface dielectric losses in the cavity, it was necessary to have a smooth lead plated surface free of oxide or other films. Lead oxidizes very easily and therefore great precautions were necessary during the plating process and during storage and use, to prevent

the cavity surface from being contaminated.

The cavity was machined out of OFHC copper. The machined cavity was first polished with fine sandpaper to remove the machine marks and then sandblasted with # 36 grit to create uniform roughness. The sandblasting was found to improve the uniformity of the final lead plated surface.

Figure 3.1 shows a block diagram of the entire plating process. Distilled and deionized water was used throughout the process. Each cavity part to be plated was held by means of a copper wire. The part was first degreased to remove any organic contamination. It was then electropolished in # 200 Electroglo polishing solution. Commercial lead was used for cathodes. The electropolishing was done just long enough to get a visibly clean copper surface.

The electropolished part was electroplated after a ten second pickling process. The formula for the plating solution is as follows:

Lead Fluoborate (50%)	800 ml
Boric Acid Powder	144 ml
Fluoboric Acid (50%)	266 ml
Water	2570 ml
Animal Glue	0.054 oz

High grade Baker and Adams chemicals were used. The lead anodes used for the plating were 99.999% pure. The plating anodes were occasionally cleaned by dipping in 25% Fluoboric

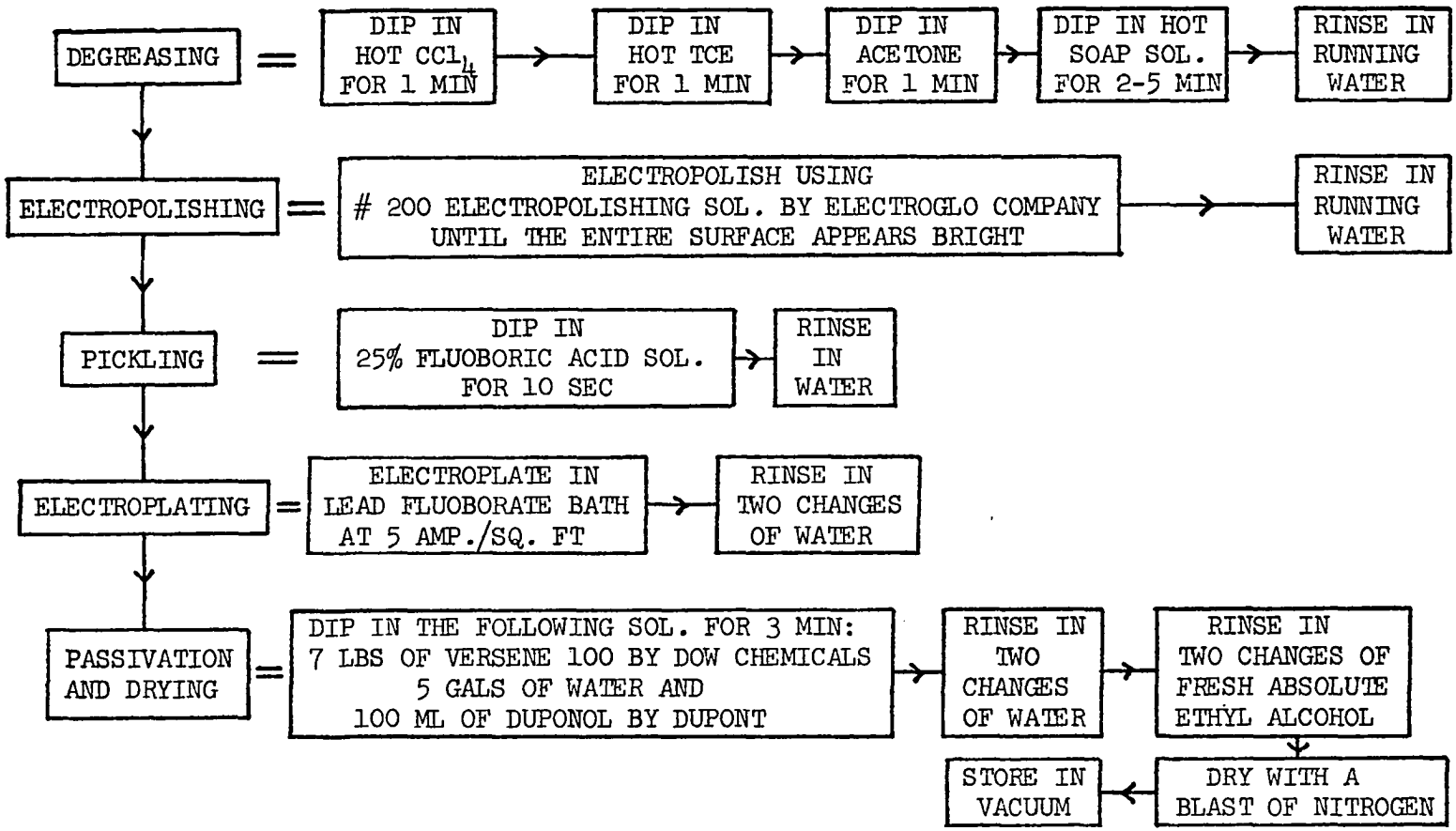

FIGURE 3.1 BLOCK DIAGRAM OF LEAD ELECTROPLATING PROCESS

acid and then scrubbing with a nylon brush.

Before starting to plate the different parts of the cavity, the lead fluoborate bath was plated out for three to four hours on a piece of copper wire at high current density. This gives the anodes an etched appearance and deposits the impurities of the plating bath on the copper wire. Before inserting any copper cathode into the plating solution a small voltage was applied to the electrodes to prevent the copper from dissolving into the plating solution. In order to achieve a more uniform plating, several anodes were used in the plating tank depending on the geometry of the part to be plated. Each part of the cavity was plated at a rate of 5 amp./ft^2 for 13 minutes to get a plating thickness of about 4 microns.

The electroplated piece was rinsed in two changes of water and then passivated in a solution of Versene and Duponol for about 3 minutes. After passivation, the cavity part was rinsed quickly in two changes of water, followed by two changes of absolute ethyl alcohol. It was then quickly dried with a jet of nitrogen. This process of passivation and drying is very important in obtaining a stain free lead plated surface. Since lead oxidizes very easily, the lead plated cavity was stored under a vacuum when not in use. When in use, the cavity was always in a helium atmosphere.

Cavity Design

A right circularly cylindrical cavity, resonant in the TE_{011} mode, is most suitable for the purpose. The currents in this mode are circumferential and they vanish around the ends of the cylindrical wall. Since no currents flow from the cylinder to the end surfaces, such a cavity can be constructed in three separate parts, the cylinder and the two end plates, without introducing spurious losses. This greatly simplifies the machining and the lead plating of the cavity. In addition, the TE_{011} mode has zero electric field everywhere on the surface. This minimizes any surface dielectric losses which might occur in the surface film.

The TM_{111} mode is degenerate with the TE_{011} mode for a right circularly cylindrical cavity. To prevent any energy from being coupled to the TM_{111} mode, it must be eliminated by suitably altering the geometry of the cavity. After having tried several designs, the cavity design shown in Figure 3.2 was found to give the best results. The circumferential cut around the edge of one of the end plates lowers the frequency of the unwanted TM_{111} mode without affecting the TE_{011} mode[31]. Thus there were no currents crossing the mechanical joints at the resonant frequency of the TE_{011} mode, and the corresponding losses were eliminated. The resonant frequency of this cavity was 12 GHz for the TE_{011} mode and its Q_o is given by[32]

$$Q_o = 779.6215/R_s \qquad (3.1)$$

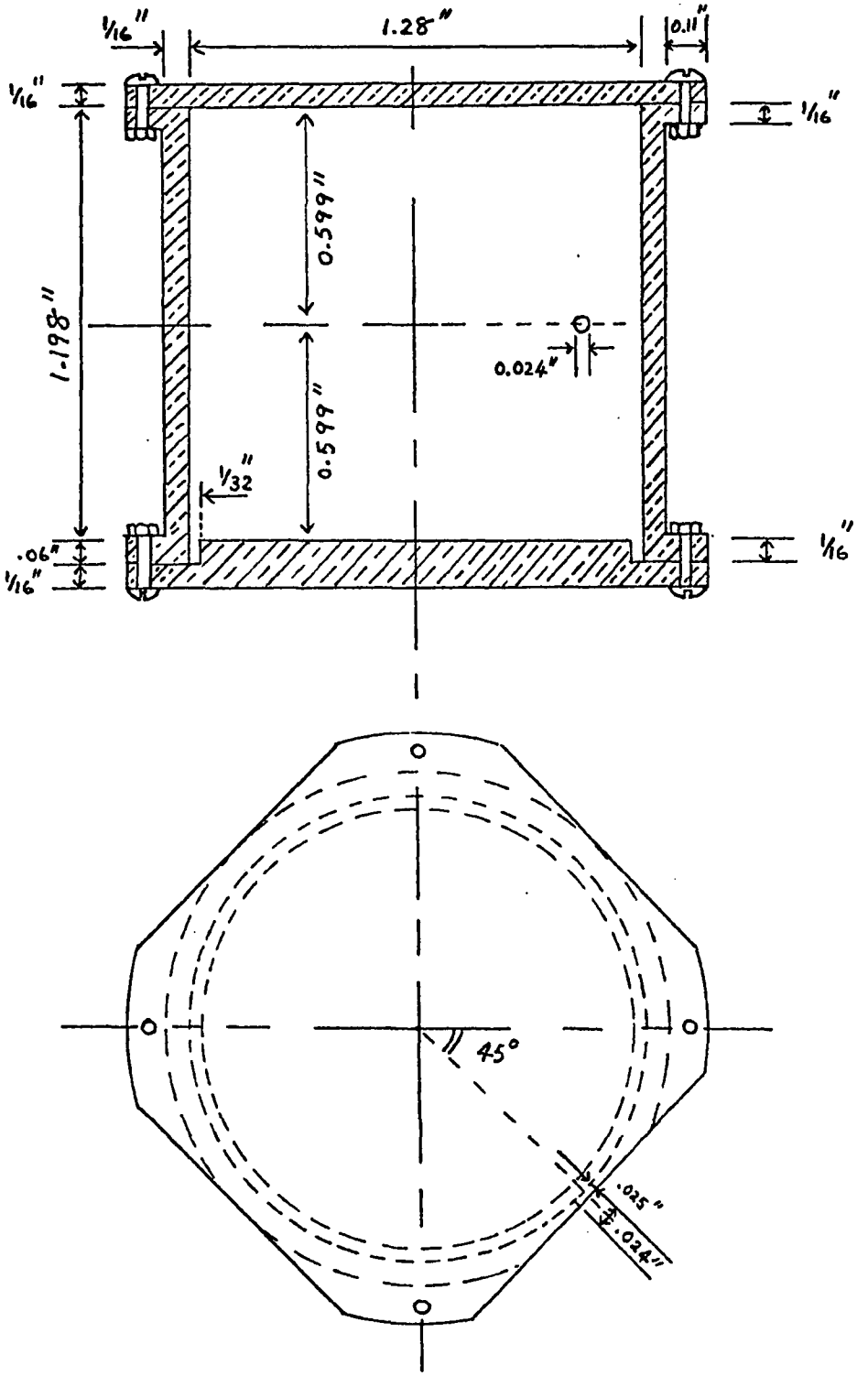

Figure 3.2 Cavity design

Coupling Mechanism

To measure the Q of a cavity, it must be coupled to external circuits. Since the electric field is zero over the entire cavity surface for the TE_{011} mode, coupling to it must be magnetic. This was achieved by means of an iris connecting the cavity with a rectangular waveguide as shown in Figure 3.3. The iris was made very small in order to maximize the radiation Q, Q_r, of the cavity. Q_r was calculated to be 4229.97×10^6.

Since the Q of the cavity was expected to vary over at least an order of magnitude, it was found necessary to have a variable coupling mechanism[32]. This was achieved by means of a copper wire closed loop suspended on a movable teflon arm in the waveguide as shown in Figure 3.3. The plane of the loop was made perpendicular to the axis of the cavity. The insulation of the copper wire was not removed except at the ends, to make a solder joint. The amount of energy coupled to the cavity could be controlled by remotely varying the penetration of the loop into the iris. During a measurement, it was never necessary to lower the loop within the cavity. This minimized the coupling losses.

Microwave Equipment and the Procedure for Measuring Q_o

A. Method of Log Decrement. This method was used when Q_o was less than 20×10^6. Figure 3.4 shows the block diagram

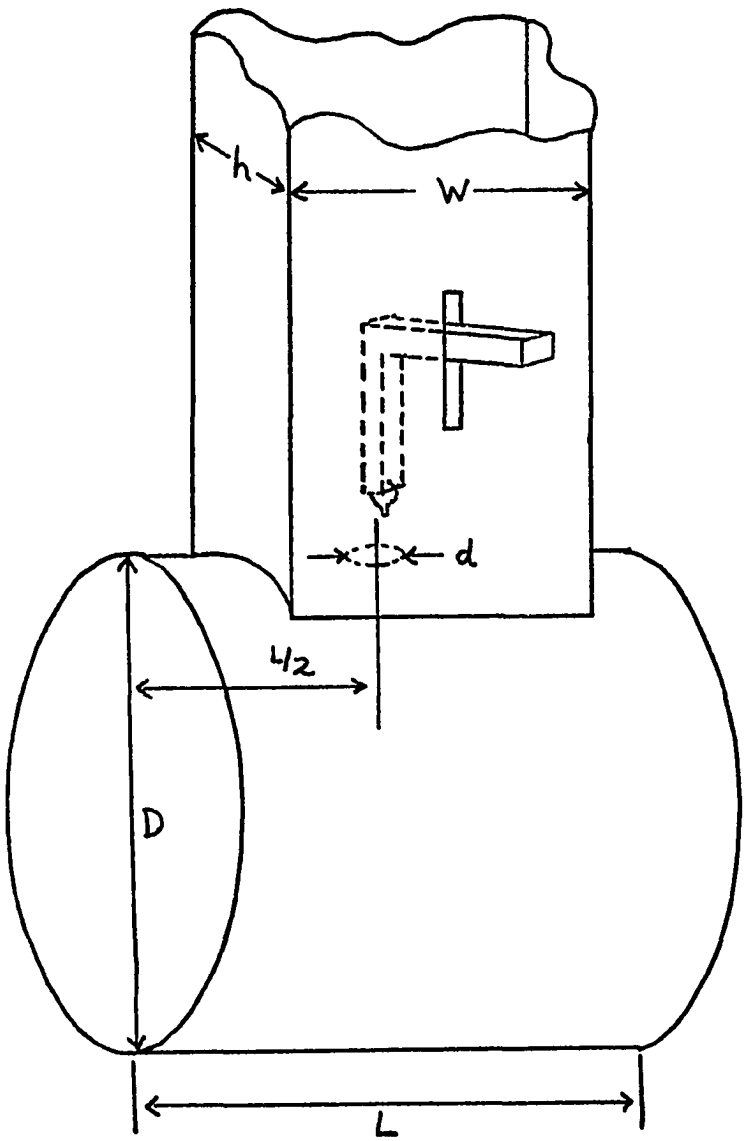

Figure 3.3 Coupling mechanism

of the microwave apparatus used. The cavity was coupled to a rectangular waveguide by a single iris between the end of the waveguide and the cylindrical section of the cavity. The iris is placed at the magnetic field maximum of both the cavity and the waveguide. Previous researchers who have used a cylindrical superconducting cavity, have placed the iris in one of the end plates of the cavity.

The measurement was performed by pulsing the r.f. energy going to the cavity under test. The PIN switch turns the microwave power on for some convenient length of time. It also initiates the linear sweep for the oscilloscope where the transient signal from the cavity is observed. During the build up process the fields in the cavity are established by means of forced oscillations induced by the oscillator. When the r.f. power from the oscillator is cut off by the PIN switch, the fields in the cavity decay exponentially with a time constant τ. The r.f. fields in the cavity are detected by a microwave diode 1N23C, and the envelope of the decaying fields is observed on the scope. This time constant is related to the loaded Q, Q_ℓ, as in equation 3.2.

$$Q_\ell = \pi f \tau \qquad (3.2)$$

where f is the resonant frequency of the cavity.

Figure 3.6 shows a typical reflected power waveform for the coupling coefficient $\beta \ll 1$. P_i is the power incident on the cavity and P_r is the power reflected from the cavity.

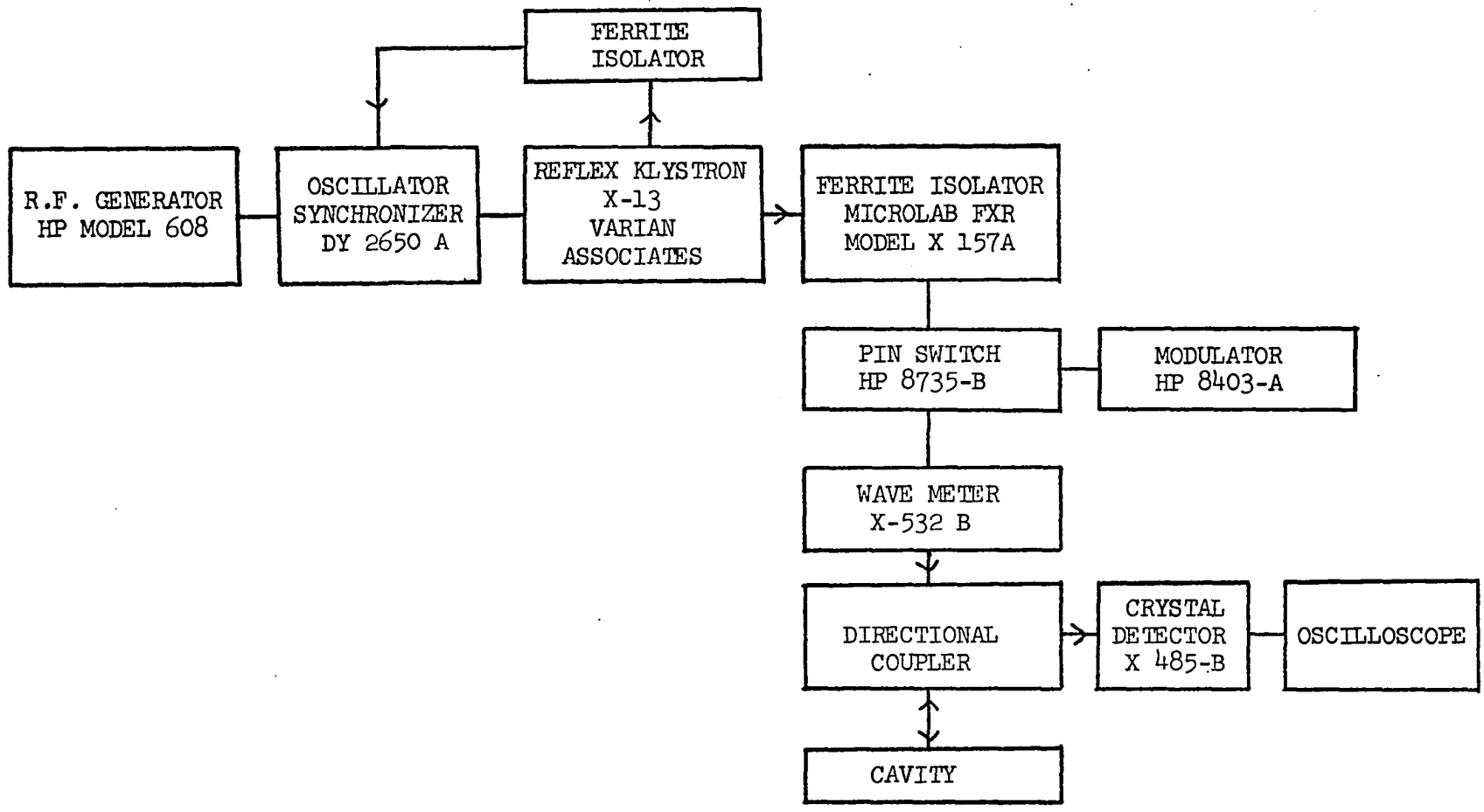

FIGURE 3.4 BLOCK DIAGRAM OF THE MICROWAVE APPARATUS

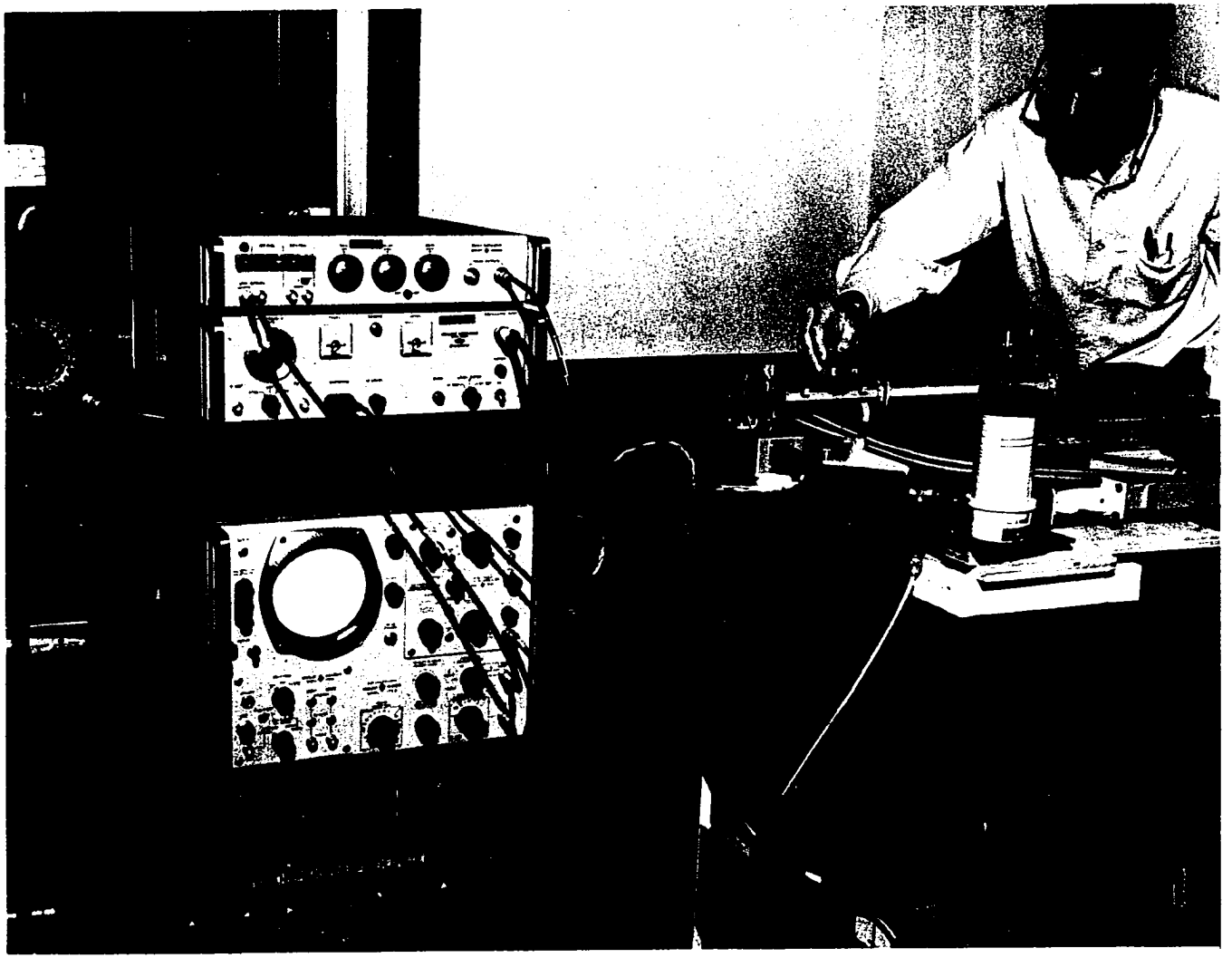

FIGURE 3.5 MICROWAVE EQUIPMENT

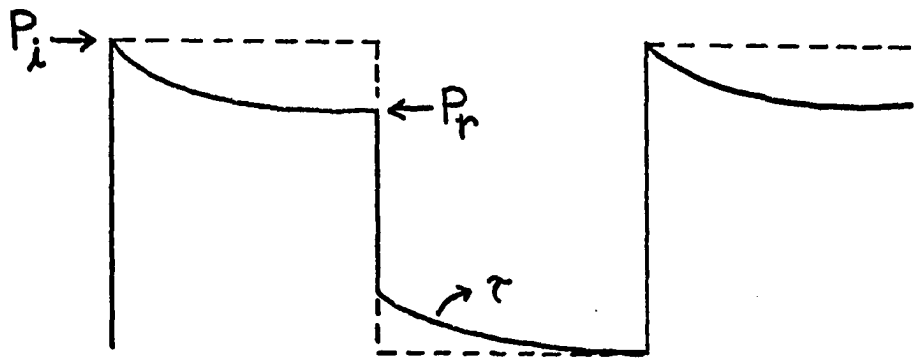

Figure 3.6 Reflected power waveform for $\beta << 1$

$$P_r/P_i = (1-\beta)^2/(1+\beta)^2 \qquad (3.3)$$

$$\text{and } Q_o = Q_\ell(1+\beta) \qquad (3.4)$$

if losses corresponding to Q_d and Q_m are negligible. The value of β could be determined from equation 3.3 by measuring P_r and P_i. All the measurements in this research were carried out with $\beta \ll 1$, by appropriately reducing the amount of energy coupled to the cavity. Therefore,

$$Q_o = Q_\ell \qquad (3.5)$$

$$\text{and } R_s = G_o Z_o/\pi f \tau \qquad (3.6)$$

From equation 3.6 it is apparent that R_s is inversely proportional to τ if the measurement is carried out with $\beta \ll 1$. Therefore, from equation 2.4,

$$1/\tau = mP(t) + c \qquad (3.7)$$

$$\text{where } m = \pi f m'/G_o^2 Z_o \text{ and } c = \pi f c'/G_o^2 Z_o$$

It is necessary that the frequency of the oscillator remain constant during the time needed to complete a measurement. Frequency fluctuations affect the level of energy build up in the cavity causing corresponding fluctuations in the trace of the decay curve presented on the oscilloscope screen. Thus, multiple traces appeared on the scope screen making it difficult to distinguish one trace from another. This problem was solved by photographing the scope screen when it had a very small number of distinct traces, and then measuring from the photographs.

B. Frequency Sweep Technique. This technique was applied

when Q_o was greater than 20 x 10^6. The same microwave apparatus as shown in Figure 3.4 was used. The PIN switch was turned off and the cavity was shock excited by a fast adiabatic passage through resonance. Here τ was the decay time constant of the eigen oscillations observed on the scope. The coupling coefficient β was again made small enough to be negligible. The problem of multiple scope traces occurred in this case also and was solved in the same manner as with the log decrement technique.

Sample Preparation

The 4% and 5% In-Sn samples were 99.999% pure obtained commercially. The 13% and 3% In-Sn samples were made in the laboratory from 99.999% pure metals. The metals were weighed on an electronic balance accurate upto 0.1 mg. The mixture of the two metals was placed in a ceramic crucible which was then heated in a quartz furnace at 250°C for 1 hour under vacuum.

The alloy formed was cleaned by immersing in a solution[37] containing: water-300 ml, $K_2Cr_2O_7$-6 grams, H_2SO_4-20 ml, NaCl (saturated solution)-12 ml, HF-80 ml and HNO_3-40 ml. It was then rolled to a thickness of about 0.5 mm in a rolling mill. Extreme care was exercised in the entire process of sample preparation to maintain the purity of the metals.

Outgassing the Quartz Tube of the Furnace

Each time before use the quartz tube was heated to a temperature of about 500°C for half hour under vacuum. It was then filled with nitrogen gas and allowed to cool. When the tube came to room temperature, the material to be heated was inserted in it. The tube was at once evacuated and then the furnace was turned on to the desired temperature.

Annealing of the Samples

The annealing was done under vacuum at 200°C for 3%, 4% and 5% In-Sn samples and at 70°C for 13% In-Sn sample. The quartz tube in which the samples were annealed was outgassed by the procedure described above each time before use. This process greatly reduced the oxidation of the alloy specimens.

Temperature Control of the Superconducting Cavity

Figure 3.7 shows the cryostat with the microwave cavity in place. The figure also shows the rod that could be pushed in or pulled out to increase or decrease the amount of microwave power coupled to the cavity. The cavity was cooled homogeneously by direct contact with liquid helium inside as well as outside the cavity.

During the precooling, the Dewar was pressurized with helium gas and was maintained at least 5 cm above atmospheric

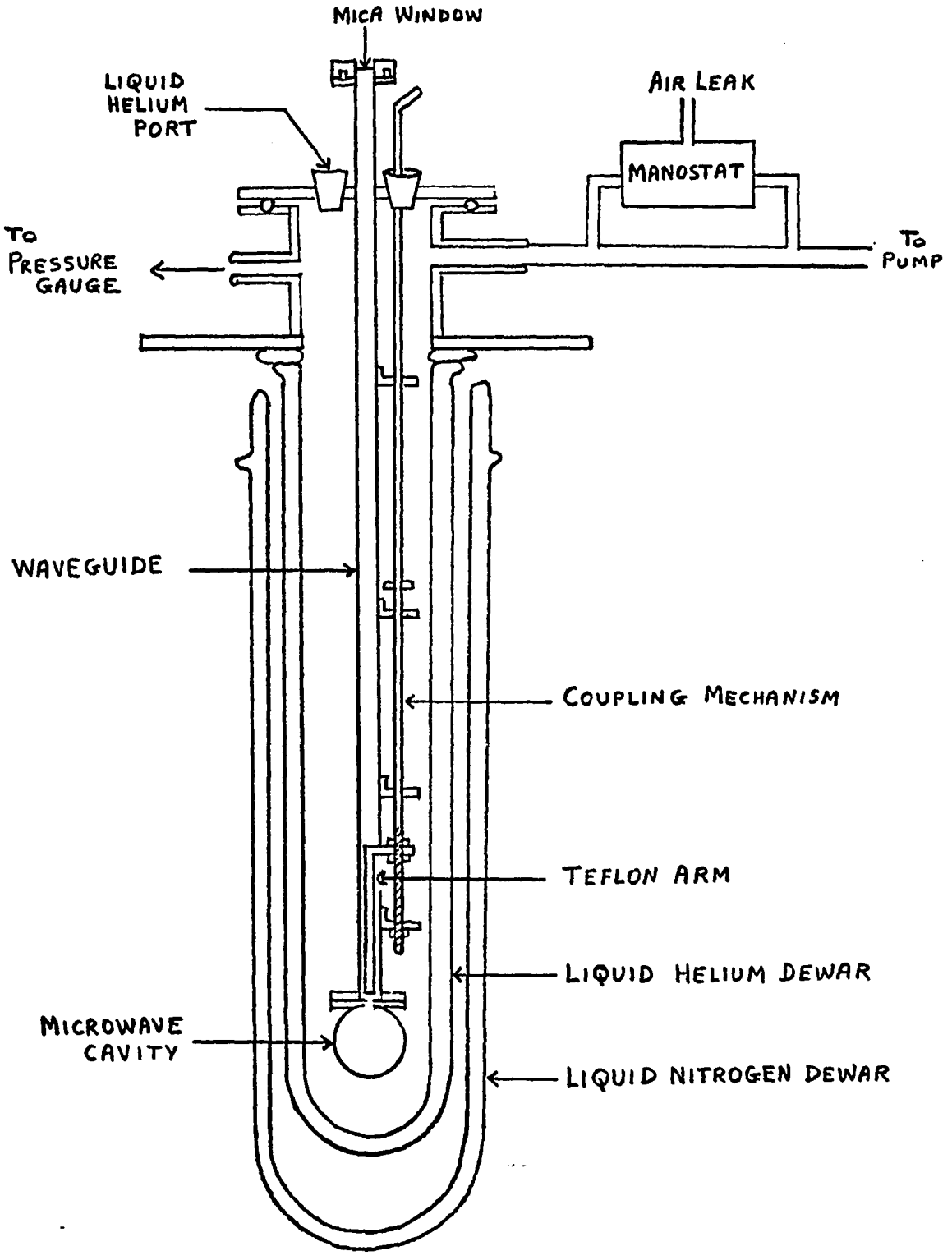

Figure 3.7 Cryostat with cavity and coupling mechanism

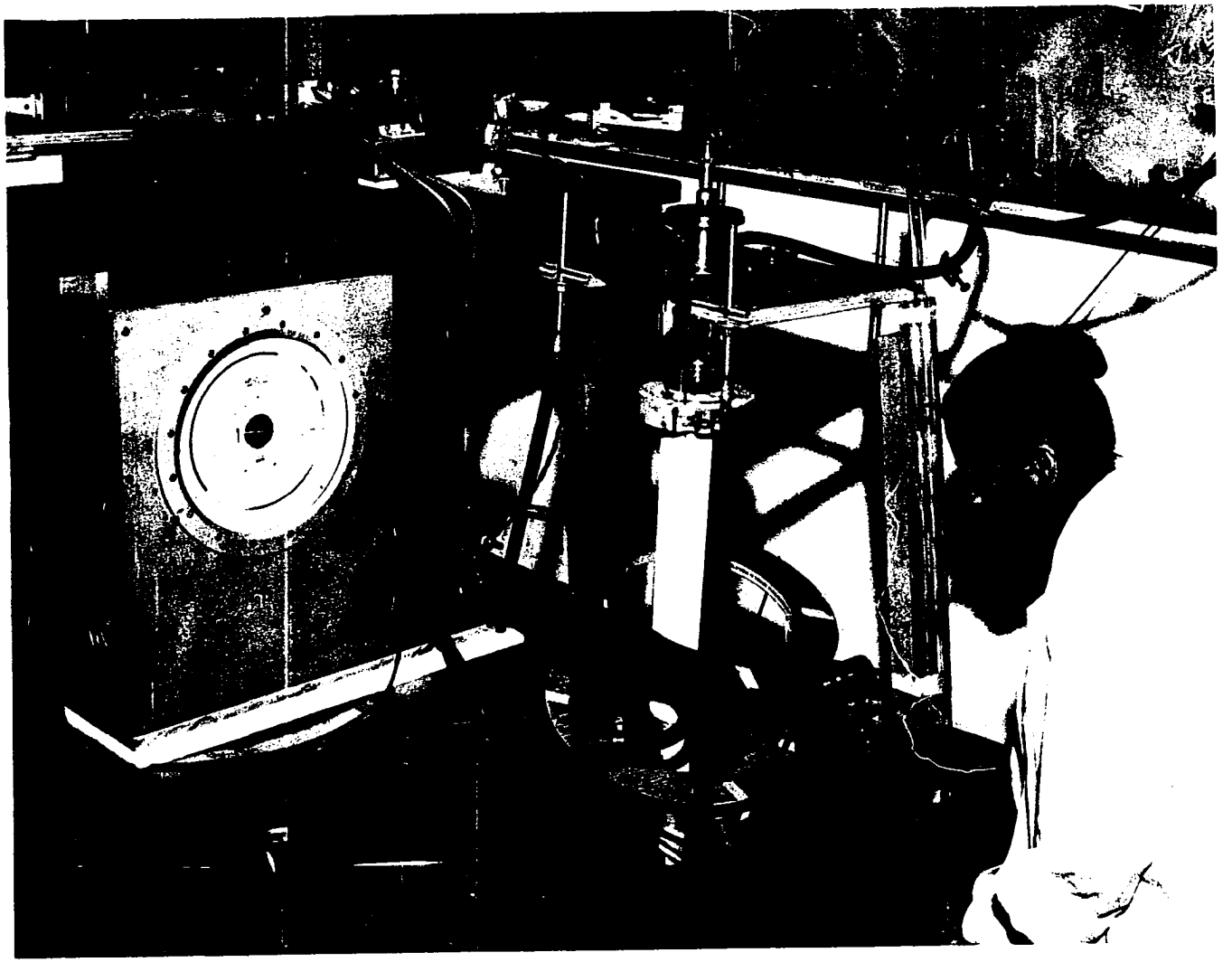

FIGURE 3.8 CRYOGENIC APPARATUS

pressure. In spite of extreme care exercised to prevent any air from leaking inside the helium Dewar, small amounts would always leak during the liquid helium transfer and turn into frost. To prevent any frost from entering the cavity via the slit in the waveguide and the coupling hole, and thus giving rise to unwanted volume dielectric losses, the cavity was covered with a fine woven nylon netting. Precooling with liquid nitrogen was continued for at least three hours before liquid helium was transferred into the Dewar.

The temperature of the liquid helium could be decreased to as low as 1.5°K by pumping on the surface of liquid helium. The pressure on the liquid helium surface was controlled and measured by a Wallace and Tiernan manostat and manometer, used in conjunction with a vacuum pump. The manostat controls the pressure in the helium Dewar by controlling an air leak to the pump. The manometer is calibrated in degrees Kelvin for helium vapour pressure so that the temperature of the liquid helium could be read directly on the manometer.

Magnetic Field Control

The external magnetic field was obtained from a Magnion Model 54122-5 electromagnet controlled by a Magnion Model HSR-1365 B Precision Magnet Power Supply. The magnetic field between the pole pieces of the electromagnet was measured with a Radio Frequency Labs Model 750 Gaussmeter.

Zero magnetic field measurements were made by reducing the earth's magnetic field to less than 0.003 gauss. This was achieved by shielding the Dewars with three layers of Co-nectic alloy and by surrounding the shielded Dewars with a Helmholtz coil pair to cancel the field component coaxial with the shield.

CHAPTER IV

RESULTS AND CONCLUSIONS

This chapter contains the results and conclusions of the data on lead and tin-indium. The quantity measured is τ, the decay time constant of the cavity. To determine τ, the exponential trace of the decay of the cavity was translated on semilog graph paper. The linear relationship between the time and the logarithm of voltage confirmed the truly exponential nature of the decay of the cavity. The quantity τ was read off directly from this linear plot on the semilog graph paper. The data are given in the Appendix.

Pure Lead Cavity

Figure 4.1 shows a plot of Q_o versus temperature for the pure lead cavity as obtained from the τ versus T data of three separate runs as given in the Appendix. The data of run # 2 show a decrease in Q_o below 3^oK. This was attributed to loss of liquid helium as was verified by the data of run # 5. The data were found to be reproducible and no sign of saturation in Q_o was observed down to 2.16^oK. The highest τ

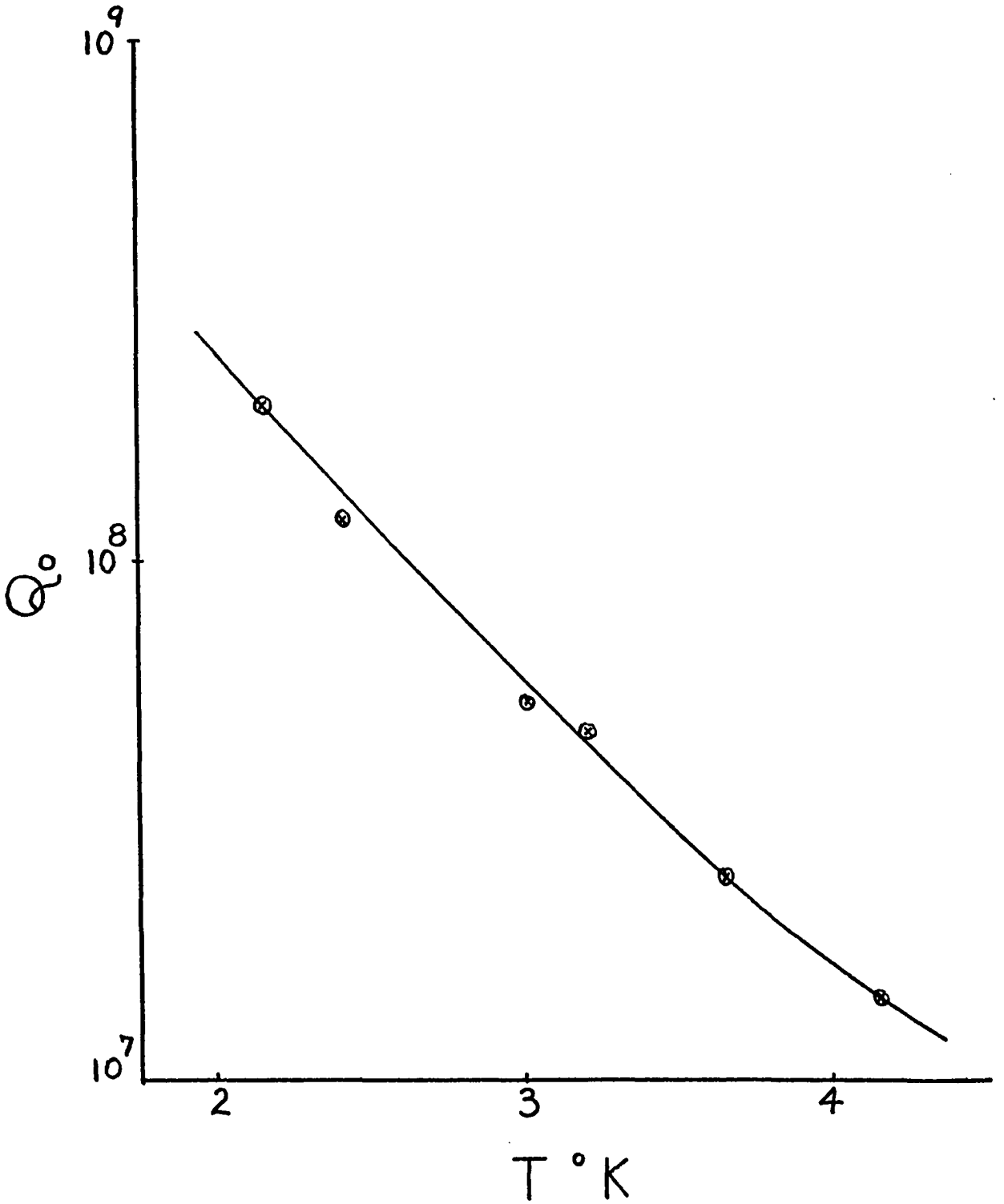

Figure 4.1 Q_o versus T for pure lead cavity

measured was 5215 μsec corresponding to a Q_o of 196.5 x 10^6 at a frequency of 12 GHz.

Figure 4.2 shows a plot of r_{exp}, the experimental reduced surface resistance versus P(t) for lead.

$$r_{exp} = \frac{R_{s,exp}}{R_{n,th}} \tag{4.1}$$

For the cavity used in this research, from equations 2.10, 3.1 and 3.2,

$$R_{s,exp} = 779.6215/\pi f \tau \tag{4.2}$$

$R_{n,th}$ is the theoretical normal surface resistance given by

$$R_{n,th} = \left(3^{\frac{1}{2}} \pi \frac{\ell}{\sigma} \left(\frac{\mu_o \omega}{4\pi}\right)^2\right)^{1/3} = 0.006045\ \Omega/\text{sq.} \tag{4.3}$$

where[31] $\sigma/\ell = 14 \times 10^{14}$ mho/m^2

It is seen that r_{exp} follows the Pippard temperature dependence as in equation 1.7, giving

$$r_{exp} = 0.0971P(t) - 0.0001795$$

The small negative intercept on the r_{exp}-axis is attributed to one of the following possibilities:

(1) Insufficient data to accurately define the intercept.

(2) Invalidity of Pippard's function at very low temperatures.

Such a negative intercept has also been observed previously[16].

Figure 4.3 is a plot of r_{exp} versus r_{AGK} as given by equation 1.4. Assuming $\Delta(0) = 1.97 k_B T_c$ following Hahn et al[31], the best straight line fit gave A = 7.326 and r_o = 0.0002826. This value of r_o corresponds to a maximum Q_o of 456.3 x 10^6.

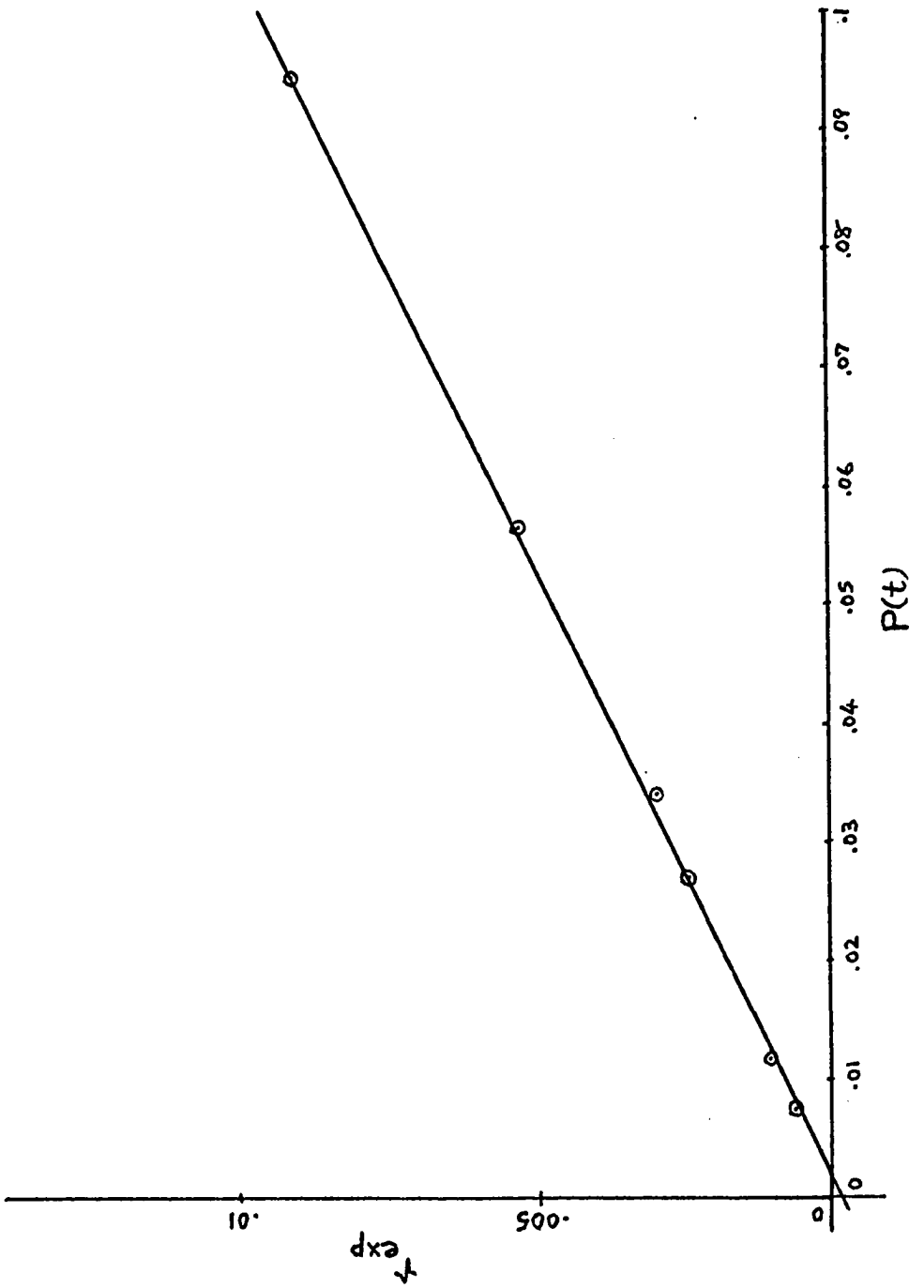

Figure 4.2 r_{exp} versus P(t) for pure lead cavity

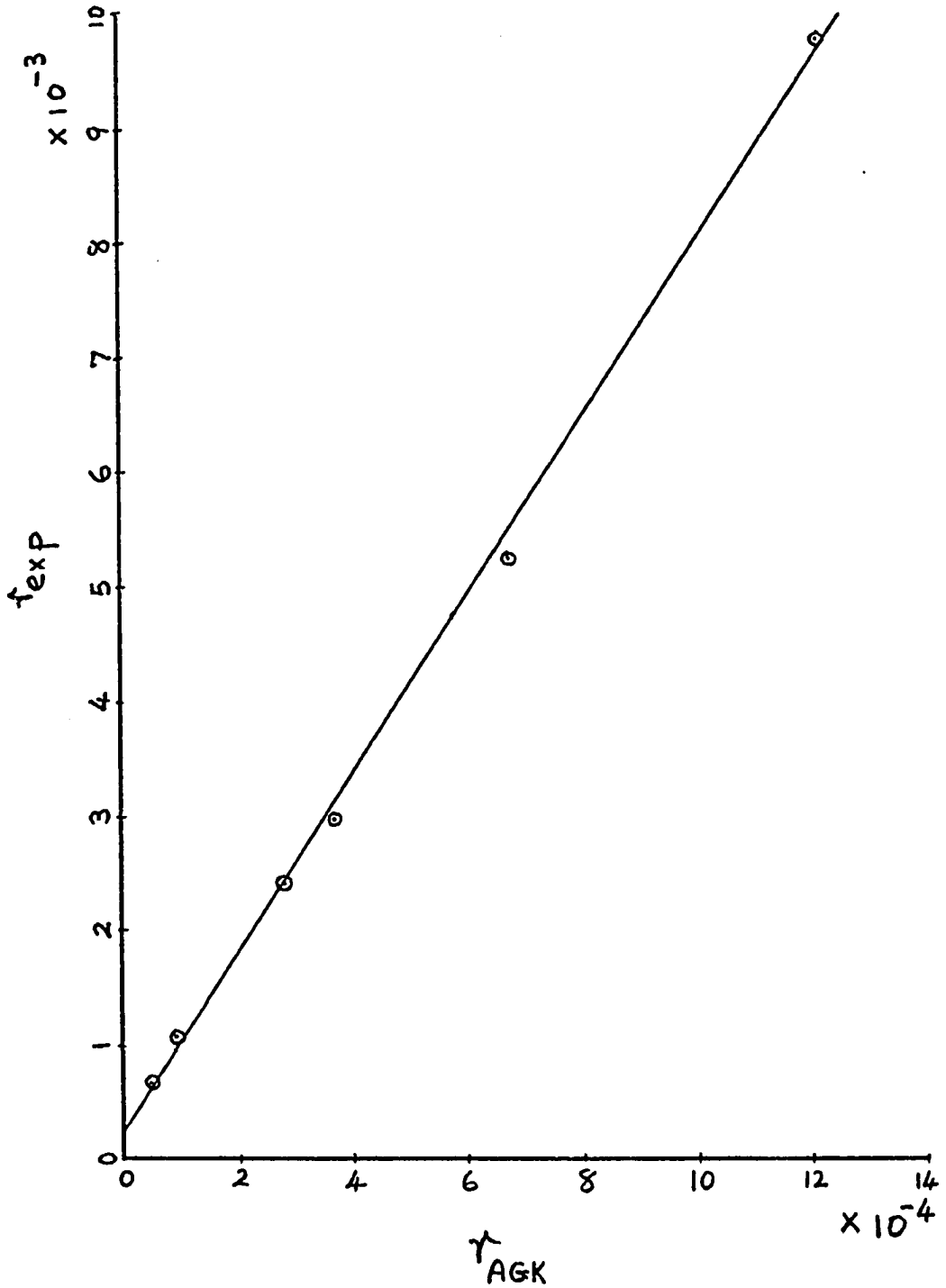

Figure 4.3 r_{exp} versus r_{AGK} for pure lead cavity

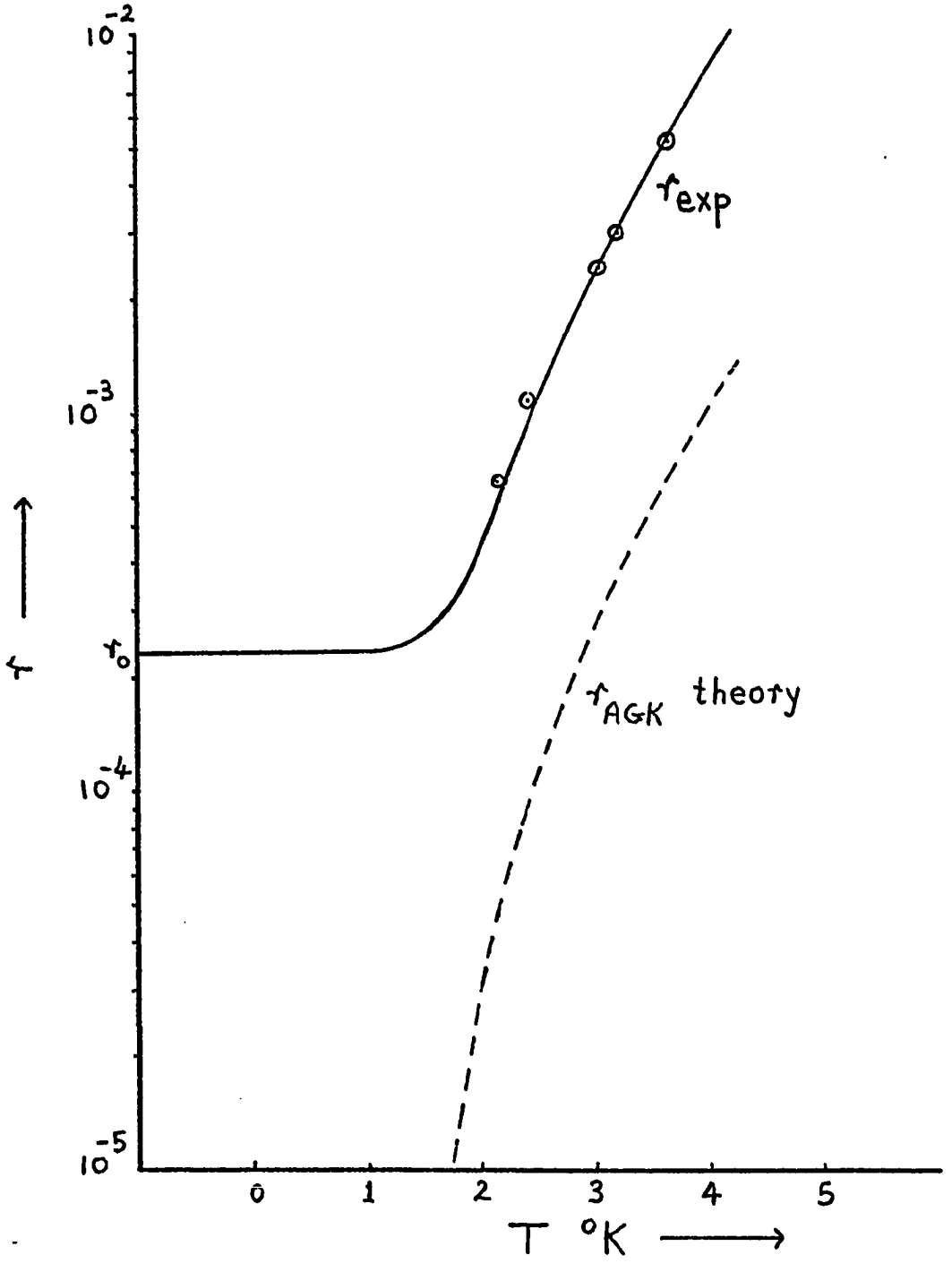

Figure 4.4 r_{exp} and r_{AGK} versus T for pure lead cavity

The experimental points, the fitted curve and r_{AGK} are shown in Figure 4.4 for comparison.

From Figure 4.1, we see that Q_o for the pure lead cavity varies by more than an order of magnitude over a temperature variation of only 2°K. Since Q_d, Q_m, Q_r and Q_c are not expected to vary over this temperature range and since r_{exp} closely follows the temperature dependences predicted by Pippard and AGK, we can conclude that for the pure lead the inequality 2.11 is satisfied and $Q_o \approx Q_\ell$.

Lead Cavity with Tin-Indium Sample

Theory for the Interpretation of Data

In order to measure the surface resistance of Sn-In, the plain lead plated end plate of the cavity was replaced by the Sn-In sample which was in the form of a thin plate. It is assumed that the superconducting surface resistance of lead is negligible in comparison with that of Sn-In. For the cavity used in this research, Q_o and R_s for Sn-In are related by[36]

$$Q_o = 9650/R_s \qquad (4.4)$$

Therefore, $$1/\tau = \pi f R_s/9650 = 39.066\times10^5 R_s \qquad (4.5)$$

In equation 4.5, substituting for R_s from equation 2.3,

$$1/\tau = \left[(A(\nu)+k\frac{H_eA_o}{H_o}5.97)P(t)+(k\frac{H_eA_o}{H_o}+r_o)\right]39.066\times10^5 R_n \qquad (4.6)$$

$$= mP(t) + c \text{ from equation } 3.7$$

where $$m = (A(\nu) + kH_eA_o5.97/H_o)39.066\times10^5 R_n \qquad (4.7)$$

$$\text{and } c = (kH_eA_o/H_o + r_o)39.066x10^5R_n \qquad (4.8)$$

This can be rewritten as

$$1/\tau = (k_1 + k_2H_eA_o)P(t) + (k_3 + k_4H_eA_o) \qquad (4.9)$$

where k_1, k_2, k_3 and k_4 are independent of H_e, t and A_o and are given by

$$\begin{aligned} k_1 &= A(\nu)\ 39.066 \times 10^5\ R_n \\ k_2 &= (k/H_o)\ 39.066 \times 10^5\ R_n \times 5.97 \\ k_3 &= r_o \times 39.066 \times 10^5\ R_n \\ k_4 &= (k/H_o) \times 39.066 \times 10^5\ R_n \end{aligned} \qquad (4.10)$$

$$\text{Then, } m = k_1 + k_2H_eA_o = k_1 + k_2 \times \text{trapped flux} \qquad (4.11)$$

$$\text{and } c = k_3 + k_4H_eA_o = k_3 + k_4 \times \text{trapped flux} \qquad (4.12)$$

Before starting the discussion of experimental results on flux-trapping it is appropriate to discuss the method of trapping flux. For flux-trapping to occur in Sn-In sample which forms the plain end plate of the cavity, the magnetic field must be applied before the Sn-In sample becomes superconducting. Two cases arise:

Case I. In this case, the magnetic field is turned on before the lead plated portion of the cavity becomes superconducting. The cylindrical section of the cavity traps all the applied flux A_TH_e where A_T is the cross sectional area of the cylinder. The magnetic field penetrates both the end plates as shown in Figure 4.5. The field at the sample is almost uniform and equal to the applied magnetic field. In this case the flux is trapped in the lead as well as the Sn-In sample. If the flux-trapping losses in lead are negligible in comparison with

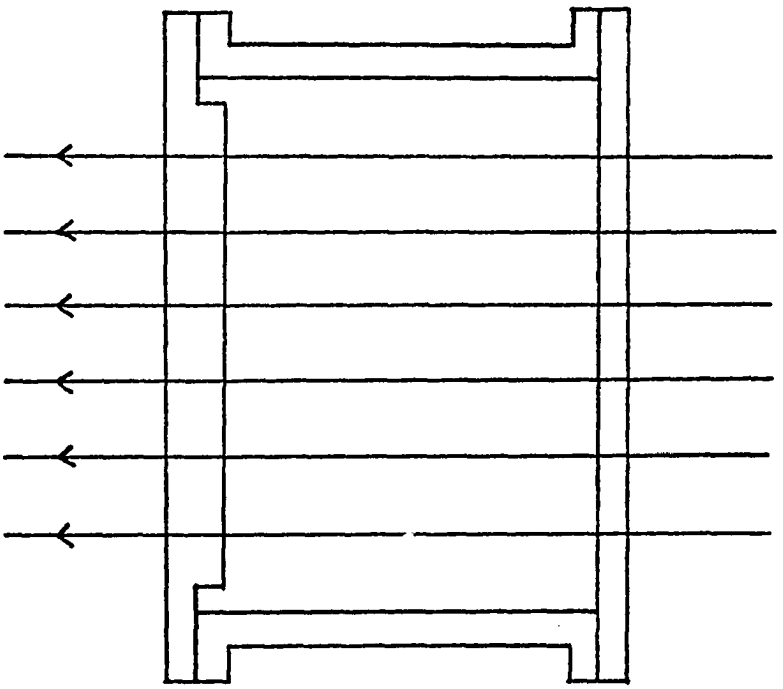

Figure 4.5 Magnetic field distribution for Case I

those in the Sn-In sample, the equations 4.10, 4.11 and 4.12 must still hold for Sn-In. However, in this case,

$$m = m_I = k_1 + k_2 A_T H_e \qquad (4.13)$$

$$\text{and } c = c_I = k_3 + k_4 A_T H_e \qquad (4.14)$$

Here $dm_I/dH_e = k_2 A_T$ and $dc_I/dH_e = k_4 A_T$ are independent of A_o. Therefore, data taken with the magnetic field applied before the lead becomes superconducting cannot be useful in studying the variation of A_o with impurity concentration and/or annealing time. However, it is shown that Case I is useful in verifying the validity of the theory developed for the Case II which follows.

Case II. In this case, the magnetic field is turned on after the lead plated portion of the cavity becomes superconducting but before the Sn-In sample becomes superconducting. The magnetic field distribution is much as shown in Figure 4.6. Because of the non-uniform magnetic field, the flux trapping will now occur over a range of temperatures. Also the magnetic field distribution will change while the flux trapping is taking place but will remain radially symmetrical at all times. As the temperature is lowered, more and more flux will be trapped until a temperature is reached when the flux trapping in the sample is complete. It is assumed here, as justified by experiment, that over the temperature range of measurements, $t < 0.8$, the total trapped flux is not a function of temperature. The magnetic field of the trapped flux can be expressed as

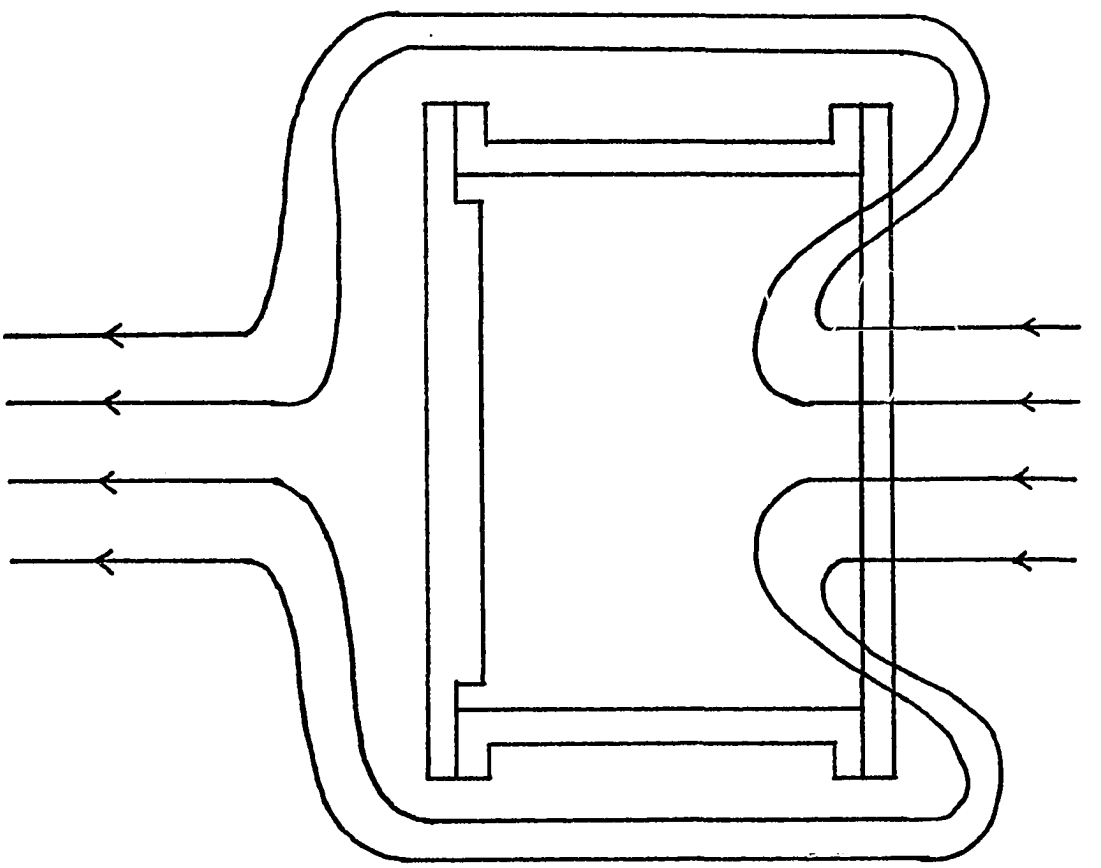

Figure 4.6 Magnetic field distribution for Case II

$$H(r) = H_e G(r) \tag{4.15}$$

where H_e is the temperature independent uniform applied magnetic field far away from the cavity,

r is the radius vector from the axis of the cylindrical cavity and

G(r) is some radially symmetrical function independent of H_e.

Assuming that the flux trapping regions are uniformly distributed over the sample, the total flux trapped by the sample is

$$\phi = \int_0^a \frac{H_e A_o}{A_T} G(r)\, 2\pi r\, dr, \tag{4.16}$$

since $H_e A_o$ in equations 4.7 through 4.12 must now be replaced by $\dfrac{A_o \int_o^a H(r) 2\pi r dr}{\int_o^a 2\pi r dr} = \dfrac{H_e A_o}{A_T} \int_o^a G(r) 2\pi r dr$

where a is the radius of the cavity. Since H_e and A_o/A_T are independent of r, the flux trapped is GA_oH_e where

$$G = \frac{1}{A_T} \int_o^a G(r)\, 2\pi r\, dr = \frac{\int_o^a H(r)\, 2\pi r\, dr}{\int_o^a H_e\, 2\pi r\, dr} \tag{4.16a}$$

is the ratio of the total flux threading the sample in the non-uniform field case to that which would thread the same if the field were uniform and equal to H_e. From equations 4.11 and 4.12, when the flux-trapping in the sample is complete,

$$m = m_{II} = k_1 + k_2 G A_o H_e \tag{4.17}$$

$$\text{and } c = c_{II} = k_3 + k_4 G A_o H_e \tag{4.18}$$

Here the linear relationship of m and c with H_e is preserved. Also dm_{II}/dH_e and dc_{II}/dH_e are proportional to A_o.

Estimation of A_o From equations 4.13, 4.14, 4.17 and 4.18, we get

$$\frac{dm_{II}/dH_e}{dm_I/dH_e} = \frac{dc_{II}/dH_e}{dc_I/dH_e} = \frac{GA_o}{A_T} \qquad (4.19)$$

The ratios $\frac{dm_{II}/dH_e}{dm_I/dH_e}$ and $\frac{dc_{II}/dH_e}{dc_I/dH_e}$ can be evaluated from the experimental data. Knowing the total sample area A_T, equation 4.19 then allows the evaluation of GA_o. Since $A_o < A_T$, a lower limit on G can be established. For the geometry of the cavity used, with a diameter to length ratio of unity, if G is assumed to be of the order of one, A_o can be estimated within an order of magnitude.

Determination of $A(0^oK)$ for a given H_e From equations 4.9 and 4.12,

$$\frac{1}{\tau(0^oK)} = c = k_3 + k_4 \times \text{trapped flux} \qquad (4.20)$$

Hence, $\frac{1}{\tau(0^oK)}$ due to trapped flux only $= c - k_3$ (4.21)

For a given Sn-In sample and a given H_e, c and k_3 can be calculated from the experimentally derived c versus H_e plots. Hence, $1/\tau$ at 0^oK due to trapped flux alone can be determined. This corresponds to losses in the normal regions of the Sn-In sample at 0^oK whose area is $A(0^oK)$. If $R_{n\lambda}$ is the surface resistance of these normal regions, then the effective surface resistance of the Sn-In sample at 0^oK is $R_{n\lambda}A(0^oK)/A_T$. From

equation 4.5, we then get

$$\frac{1}{\tau(0^{\circ}K)} \text{ due to trapped flux only} = 39.066 \times 10^{5} R_{n\lambda} \frac{A(0^{\circ}K)}{A_T} \qquad (4.22)$$

Knowing $R_{n\lambda}$, A_T and the left hand side of equation 4.22, $A(0^{\circ}K)$ can be found for a given value of H_e.

Determination of H_o and Area per Fluxoid at $0^{\circ}K$ for a given Sn-In Sample.

For Case I, $$A(0^{\circ}K)\, H_o = A_T\, H_e \qquad (4.23)$$

For Case II, $$A(0^{\circ}K)\, H_o = G\, A_o\, H_e \qquad (4.24)$$

Methods for the evaluation of $A(0^{\circ}K)$ for a given H_e and of GA_o have been described in the preceding paragraphs. Therefore, H_o can be determined either from equation 4.23 or equation 4.24.

Dividing the quantum of flux[35], 2×10^{-11} gauss m^2 by H_o directly yields the area per fluxoid at $0^{\circ}K$.

Data on 5% In-Sn Sample

Experimental measurements were made on a 5% In-Sn sample with the flux trapped as in both the cases described above. This sample was obtained commercially in the form of a 3 mil thick foil rolled out of 99.999% pure alloy. The as-rolled alloy was annealed for 24 hours at 200°C. Figure 4.7 shows the data of run # 3 taken on this sample with the flux trapped as in Case I above. The decay time constant τ was measured as a function of temperature with different applied

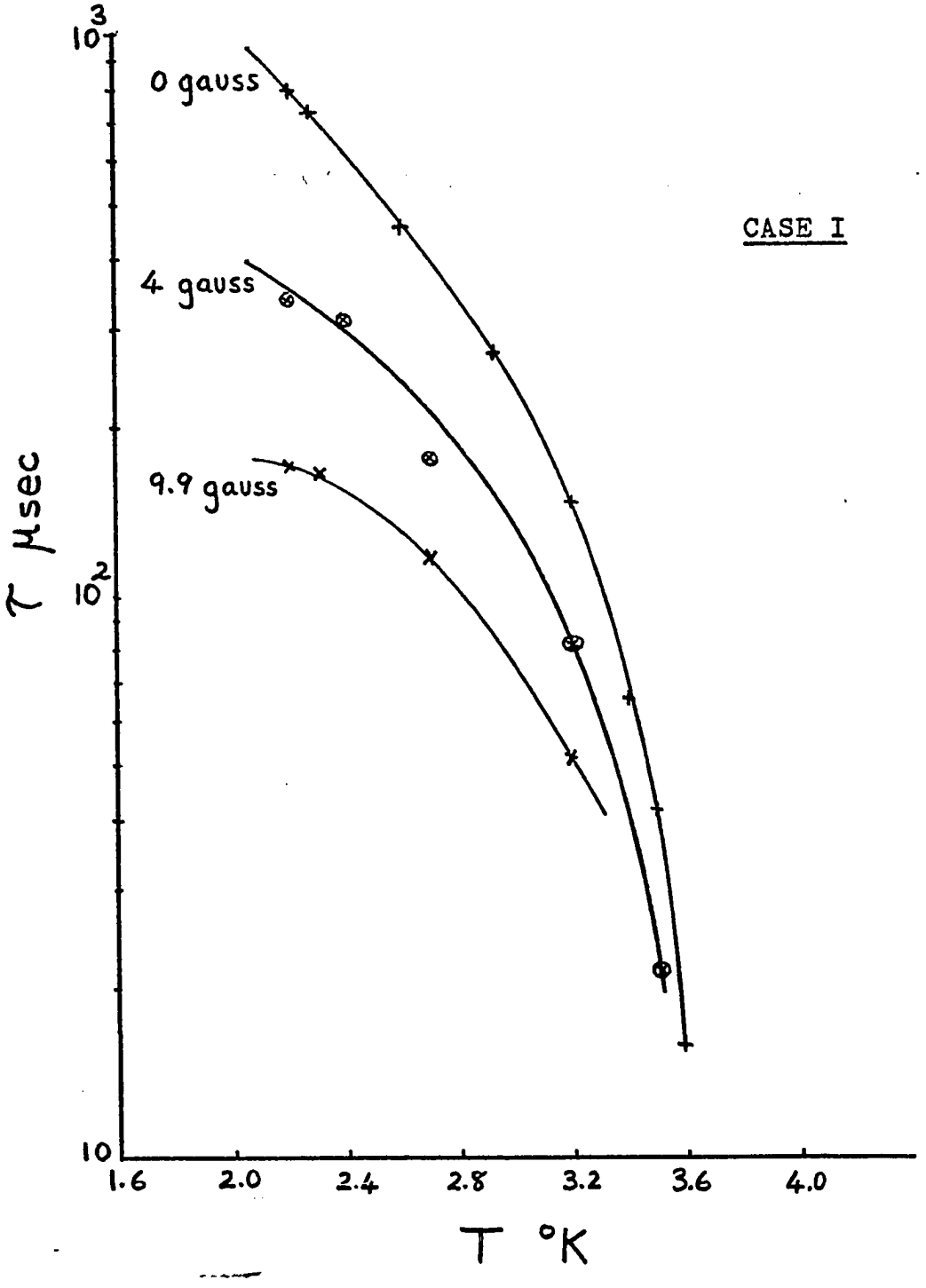

Figure 4.7 τ versus T for 5% In-Sn sample

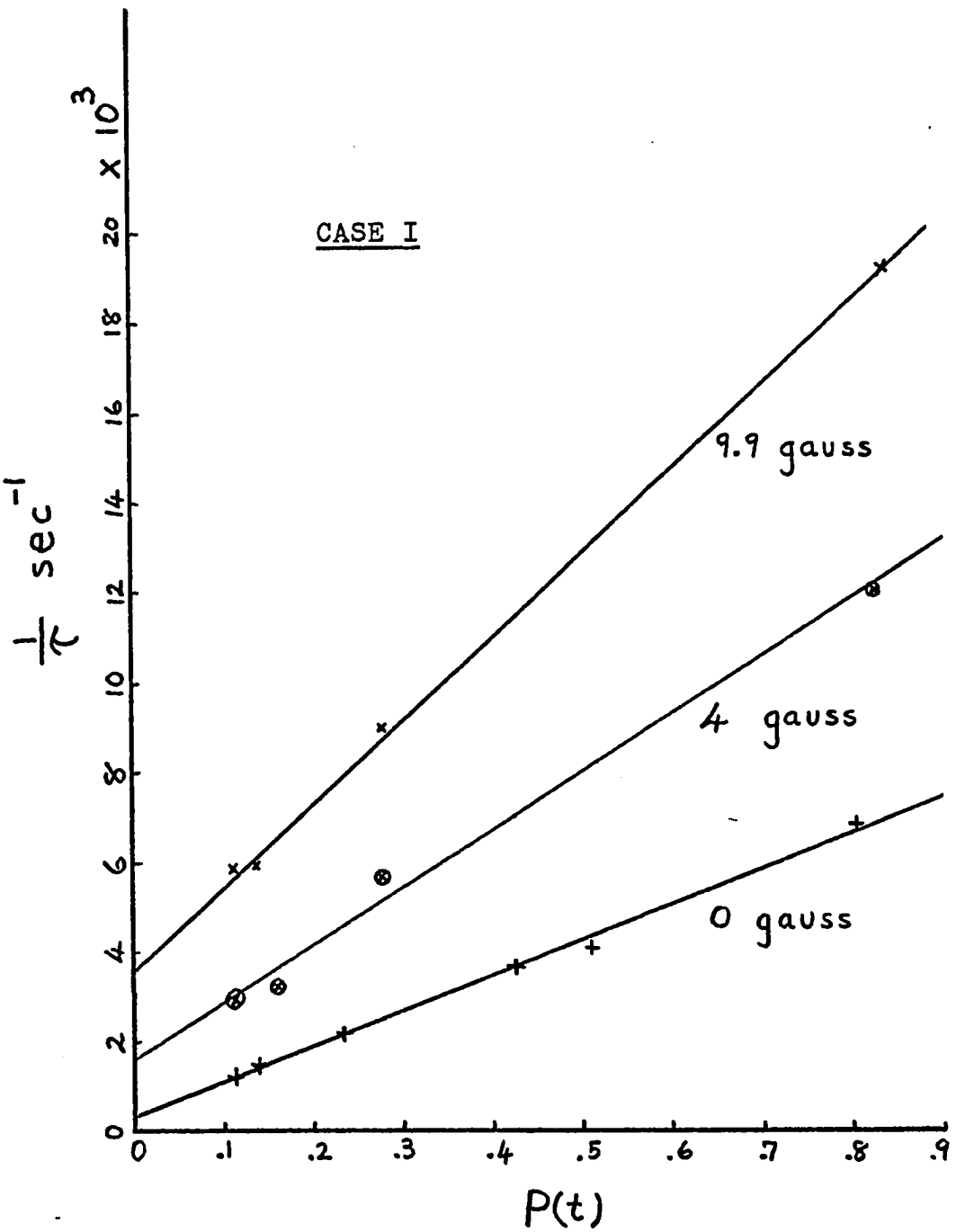

Figure 4.8 $1/\tau$ versus P(t) for 5% In-Sn sample

magnetic fields. Figure 4.8 shows the data plotted on $1/\tau$-P(t) plane with H_e as the parameter. The linear dependence of $1/\tau$ on P(t) for $H_e = 0$ gauss, in the absence of flux trapping, verifies that the losses in lead are indeed negligible as compared to the losses in the alloy over the temperature range of interest. For the data with the magnetic field $H_e = 4.0$ and 9.9 gauss the magnetic field was applied before the lead became superconducting. Hence, as described in Case I above, all the applied flux was trapped. Also in this case the flux must be trapped in lead as well as in the alloy specimen. The fact that these data follow the Pippard temperature dependence proves that even the flux-trapping losses in lead are much smaller than the flux-trapping losses in the Sn-In alloy. Figure 4.11 shows that m and c for this case are both proportional to the applied magnetic field.

A data run on the same sample was repeated, run # 4. This time the magnetic field was turned on after the lead plated portion of the cavity became superconducting, as described in Case II above. The data for $H_e = 0$ gauss was found to be reproducible. Figure 4.9 shows the data. Figure 4.10 shows the data plotted on the $1/\tau$-P(t) plane. The Pippard temperature dependence is observed up to an applied magnetic field of at least 70 gauss.

From Figure 4.11,

$$\frac{dm_I/dH_e}{dm_{II}/dH_e} = 6.83$$

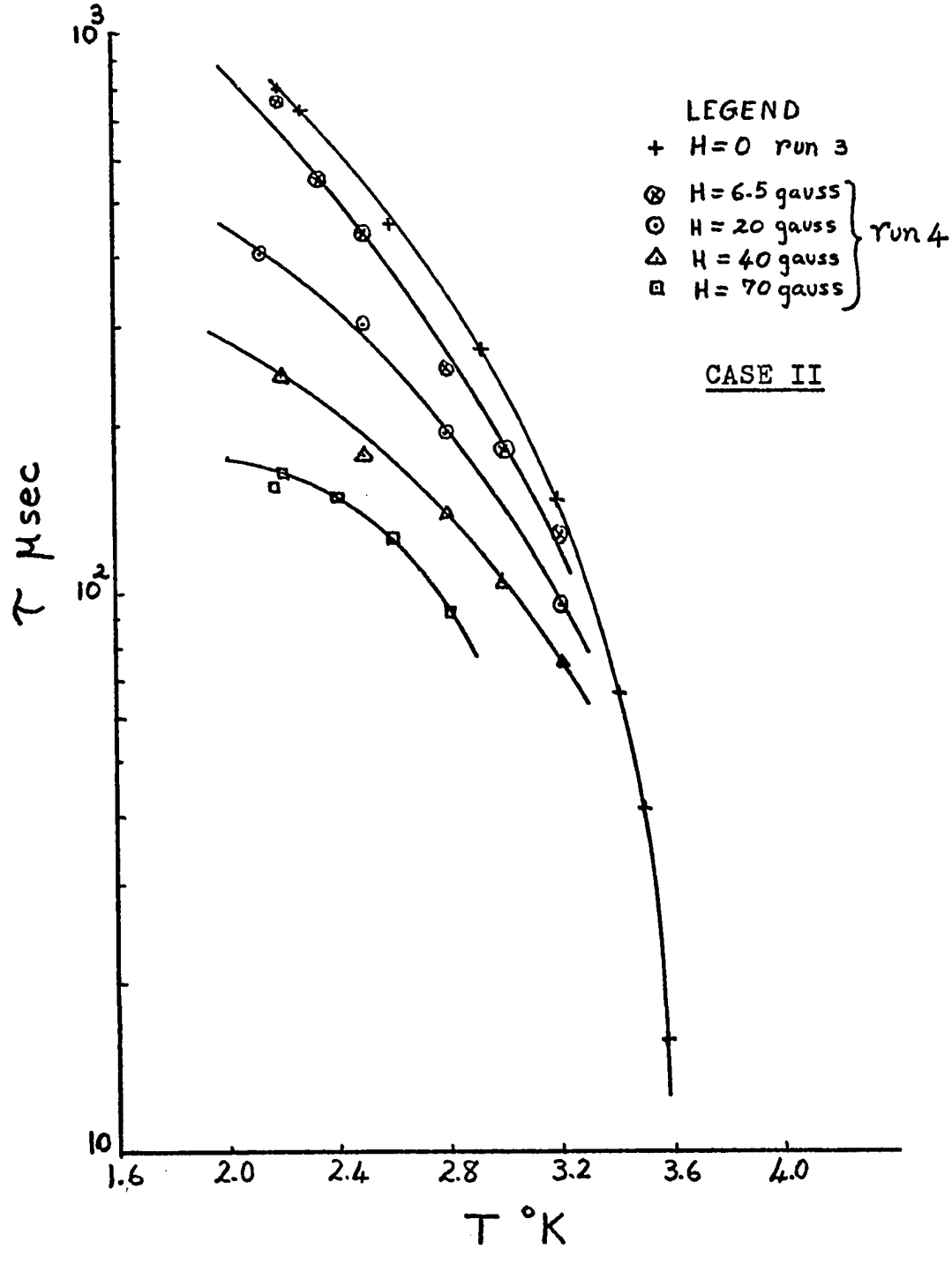

Figure 4.9 τ versus T for 5% In-Sn sample

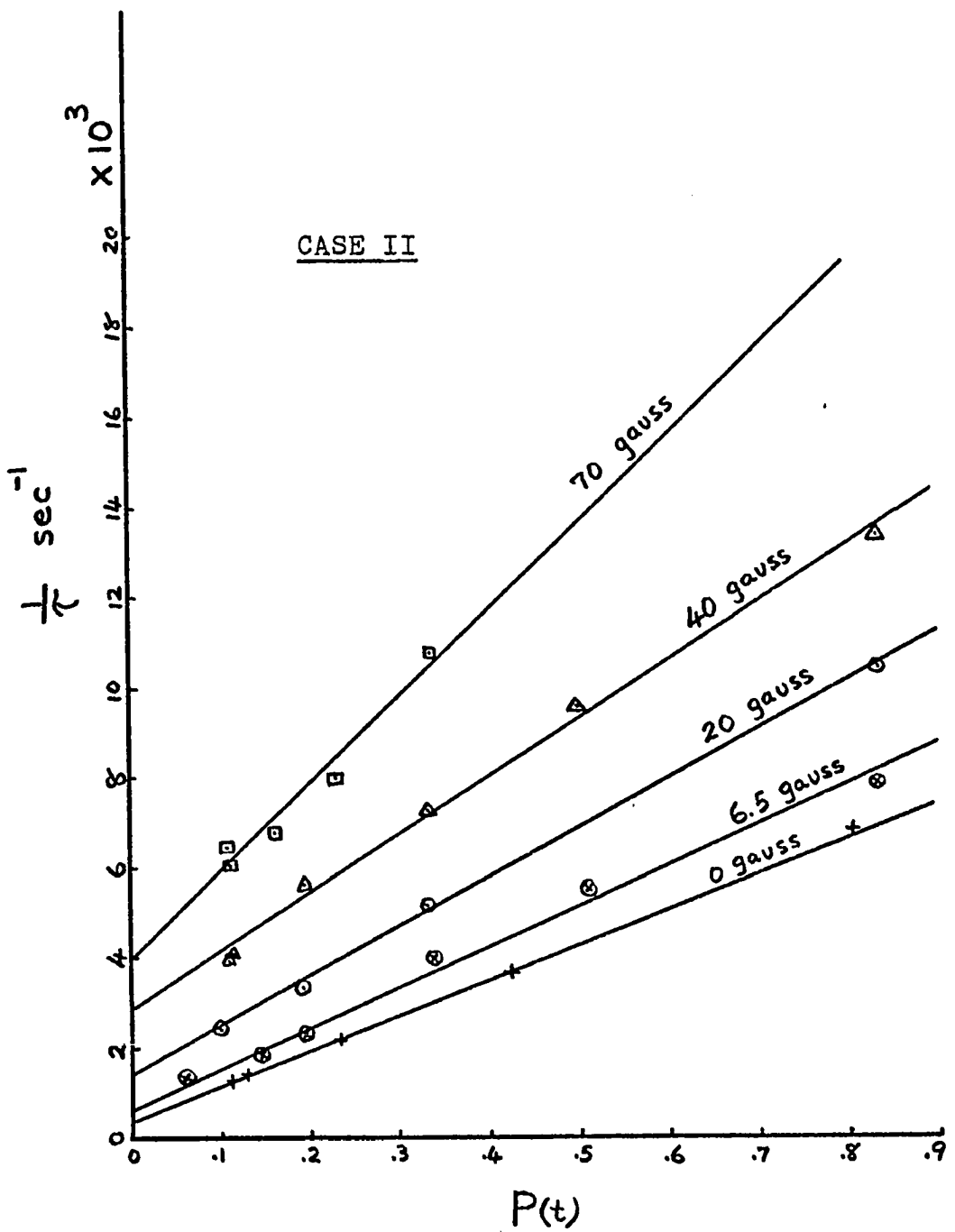

Figure 4.10 $1/\tau$ versus P(t) for 5% In-Sn sample

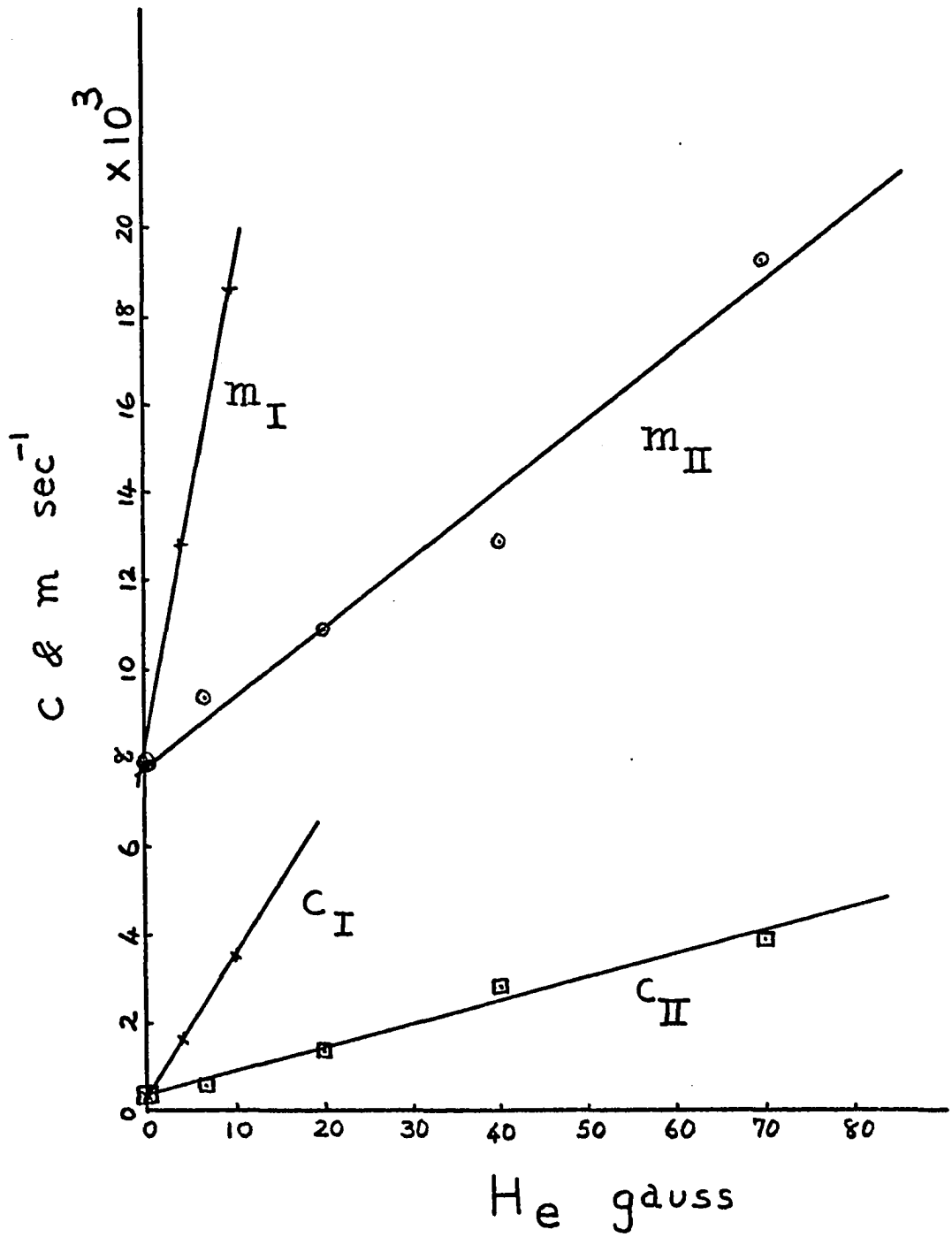

Figure 4.11 c and m versus H_e for 5% In-Sn sample

$$\text{and } \frac{dc_I/dH_e}{dc_{II}/dH_e} = 5.98$$

Using the average value of 6.4, $A_oG = A_T/6.4$. For the experimental cavity, $A_T = 8.3 \times 10^{-4}$ m^2

Thus, $$A_oG = 1.29 \times 10^{-4} \text{ m}^2$$

$$\text{and } A_o \sim 10^{-4} \text{ m}^2$$

It is therefore estimated from the experimental results that roughly one tenth of the total area of the sample traps flux at the moment of transition into the superconducting state.

Also, if we define H_{eff-1}, the effective magnetic field in Case I of flux-trapping as equal to H_eA_T/A_o and H_{eff-2}, the effective magnetic field in Case II of flux-trapping as equal H_eG, then $H_{eff-1} = 6.4 \times H_{eff-2}$ for the same applied magnetic field.

From Figure 4.11, $1/\tau(0^oK)$ due to trapped flux alone is 6451.8 sec^{-1} for H_e = 20 gauss. Therefore, from equation 4.22

$$6451.8 = 39.066 \times 10^5 \times R_{n\lambda} \times \frac{A(0^oK)}{A_T}$$

Here, $R_{n\lambda} = 0.604$ ohms/square assuming that $R_{n\lambda} = \rho/\lambda(0^oK)$ where ρ, the low temperature bulk resistivity is taken to be 3.08×10^{-6} ohms-cm following Haden and $\lambda(0^oK)$ for Sn-In is assumed to be the same as that for Sn, namely 510 Å. Knowing A_T, $A(0^oK) = 2266 \times 10^{-9}$ m^2 for H_e = 20 gauss and Case I. Hence, using equation 4.23, H_o = 7320 gauss.

From Figure 4.11, $1/\tau(0^{o}K)$ due to trapped flux alone is 1076.4 sec^{-1} for H_e = 20 gauss and Case II. Therefore,

$$1076.1 = 39.066 \times 10^{5} \times 0.604 \times \frac{A(0^{o}K)}{A_T}$$

Once again knowing A_T, $A(0^{o}K) = 378.2 \times 10^{-9}$ m^2 for H_e = 20 gauss and Case II. Using equation 4.24, H_o = 6840 gauss.

The value of H_o obtained from the data of Case I and Case II are the same within the experimental error. Using the average value of 7080 gauss for H_o, the area per fluxoid at $0^{o}K$ is 2.825×10^{-15} m^2.

The important conclusion of the results of these two runs is the linear dependence of $1/\tau$ on P(t) and of m and c on H_e for both the uniform and the non-uniform cases of flux trapping. In the flux trapping data that follow the magnetic field was applied at about $4.2^{o}K$ when the lead was superconducting.

Data on 4% In-Sn Sample

This sample was obtained commercially in the form of a 3 mil thick foil rolled out of 99.999% pure alloy. The as-rolled sample was annealed for 24 hours at $200^{o}C$. Figure 4.12 shows the plot of τ versus T for this sample with H_e as the parameter. Figure 4.13 shows the data plotted on the $1/\tau$-P(t) plane. The Pippard temperature dependence is observed up to an applied magnetic field of at least 75 gauss.

CASE II

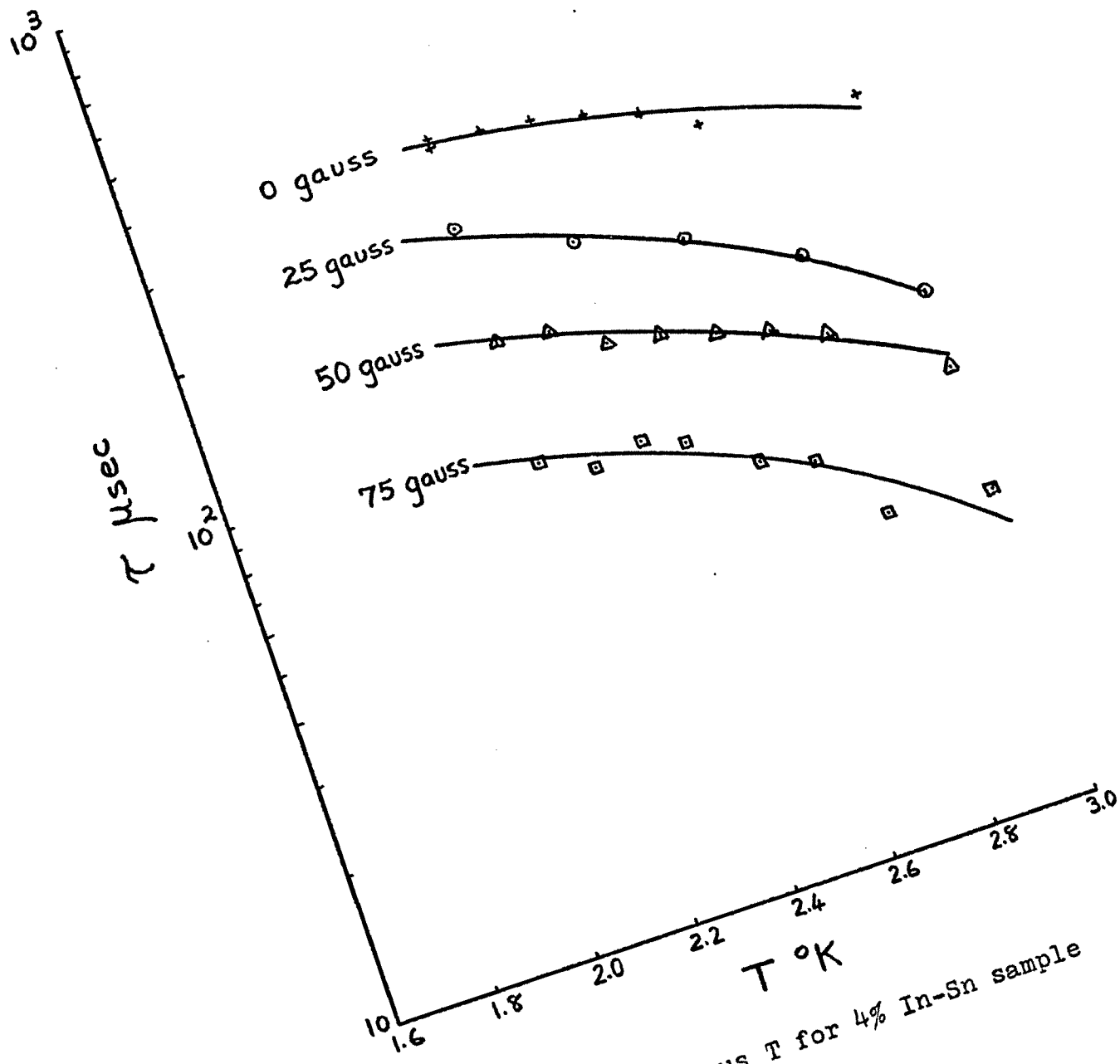

Figure 4.12 τ versus T for 4% In-Sn sample

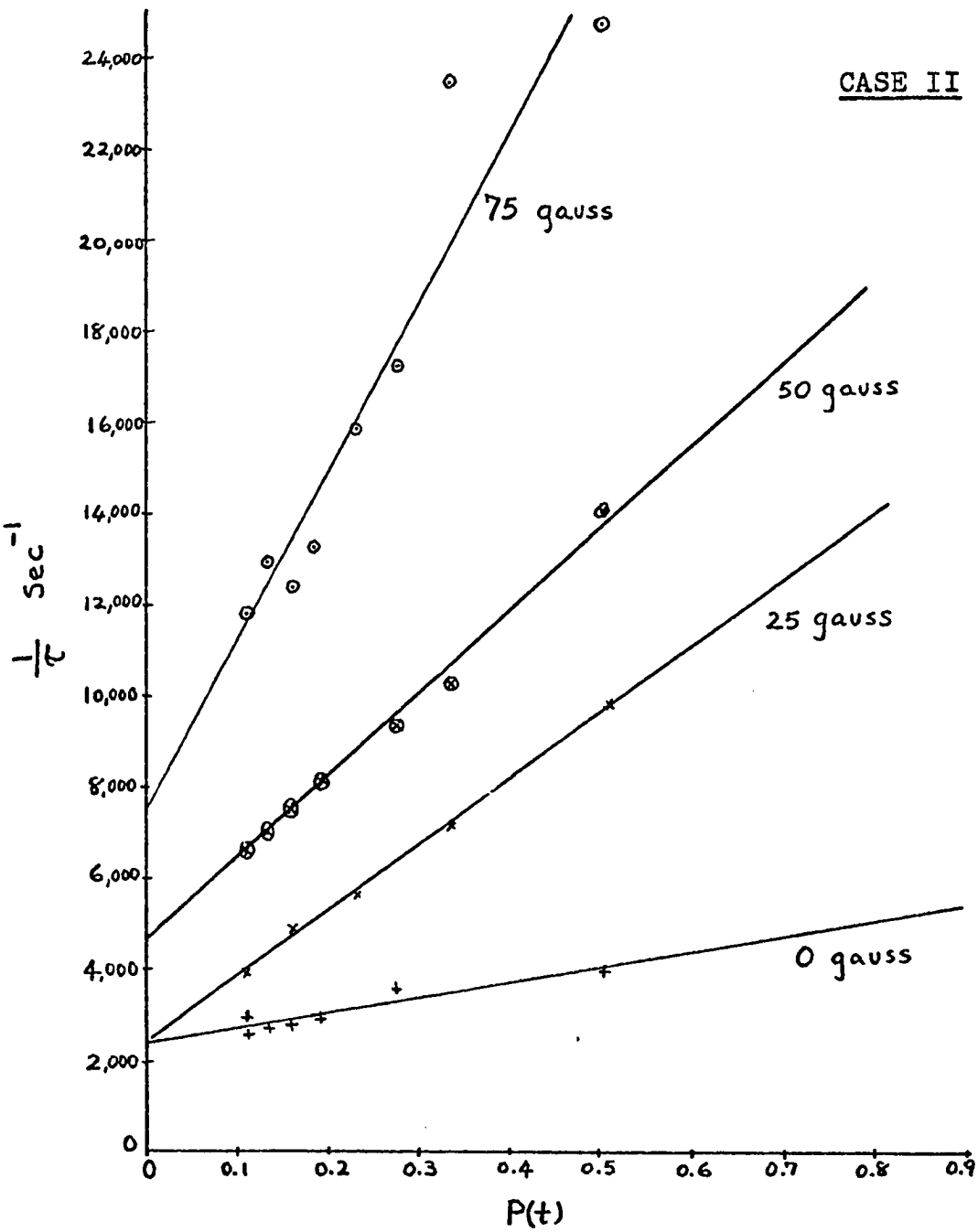

Figure 4.13 $1/\tau$ versus P(t) for 4% In-Sn sample

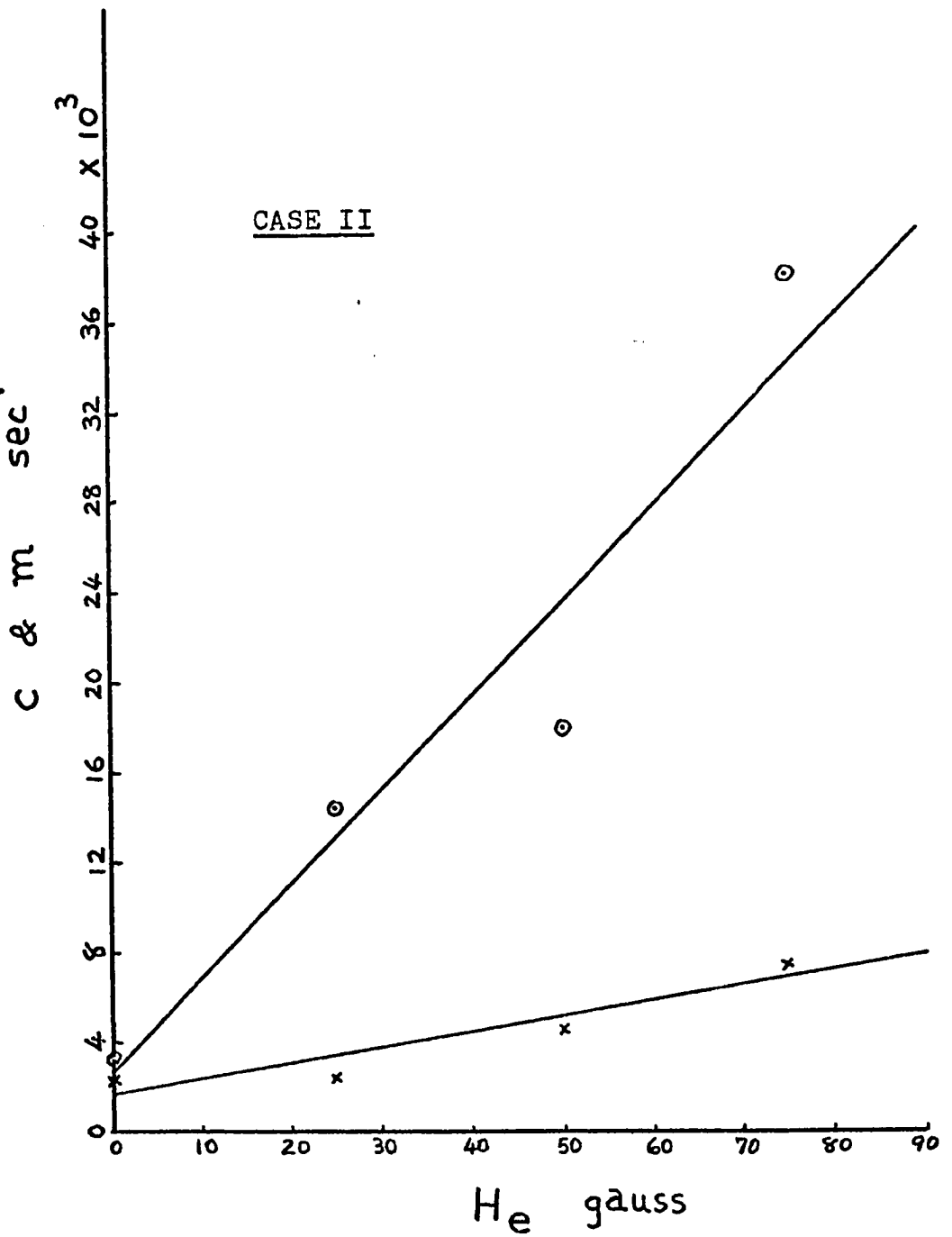

Figure 4.14 c and m versus H_e for 4% In-Sn sample

Figure 4.14 shows the dependence of m and c on H_e. dc/dH_e and dm/dH_e for this sample are much larger than those of the 5% In-Sn sample annealed for the same length of time at the same temperature. On examining the two samples visibly, the grains of the 4% In-Sn sample appeared smaller than the grains of the 5% In-Sn sample. This indicated that most of the flux-trapping occured because of the deformities rather than the impurities in the sample. It was concluded that in order to study the effect of a small change in impurity on the flux-trapping capability, the sample must be annealed for a prolonged period of time. An alternate solution could be to have a larger variation in impurity concentration. Looking at the phase diagram of Sn-In the immediate solution seemed to be γ-phase tin-indium. The γ-phase ranges over 12-24% In in Sn as compared to the δ-phase which ranges over only 0-6% In in Sn. Data were taken on a laboratory made 13% In-Sn alloy. The results are given below.

Data on a Laboratory Made 13% In-Sn Sample

This sample was made out of 99.999% pure metals. The cold-rolled sample was annealed for 29.5 hours at 70°C. The grains of this sample were visibly larger than those of the previous two samples. The data on this sample are given in the Appendix. The data were not found to be reproducible and the losses decreased with time. This alloy has a very low recrystallization temperature and is known to anneal even at

room temperature. It was concluded that this sample was annealing at a rather rapid rate at room temperature. The Υ-phase tin-indium was therefore not found to be convenient for studying the effect of impurity on flux-trapping.

Effect of Annealing on Flux-trapping

To study the effect of defects on flux-trapping, a 3% In-Sn alloy was made in the laboratory. The metals used to form the alloy were 99.999% pure. Data were taken to determine dc/dH_e and dm/dH_e as a function of the annealing time, starting with the cold-rolled alloy. Annealing was done at a constant temperature of 200°C. Figures 4.15, 4.16, 4.17 and 4.18 show the metallographs of the sample for 0, $\frac{1}{2}$, 1 and 4 hours of annealing time.

Figures 4.19, 4.20 and 4.21 show the data plotted on the $1/\tau$-P(t) plane with H_e as the parameter, for annealing periods of 0, $\frac{1}{2}$ and 1 hour respectively. The Pippard temperature dependence is observed as before.

Figure 4.22 is a plot of m versus H_e for the three different annealing times. m is found to be linear with H_e. The zero magnetic field intercepts of the straight lines in Figure 4.22 indicate that $A(\nu)$ in equation 4.7 varies in a random fashion with annealing. In reality each time after the sample was annealed it was slightly etched to clean any oxide film that may have formed on it during annealing. Thus,

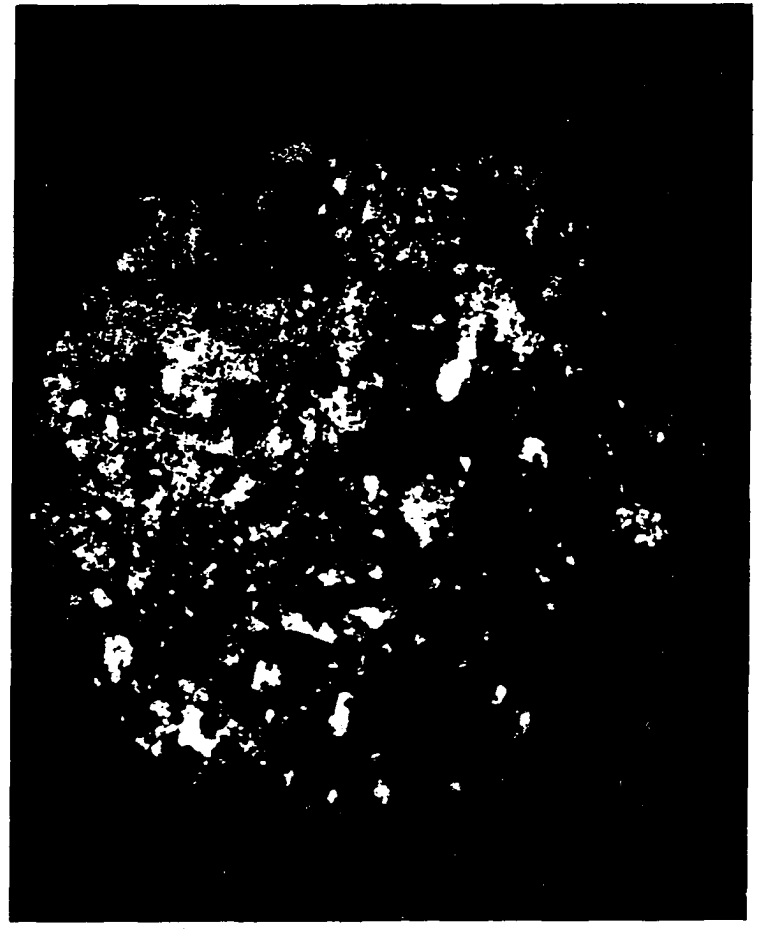

FIGURE 4.15 0 HR ANNEAL

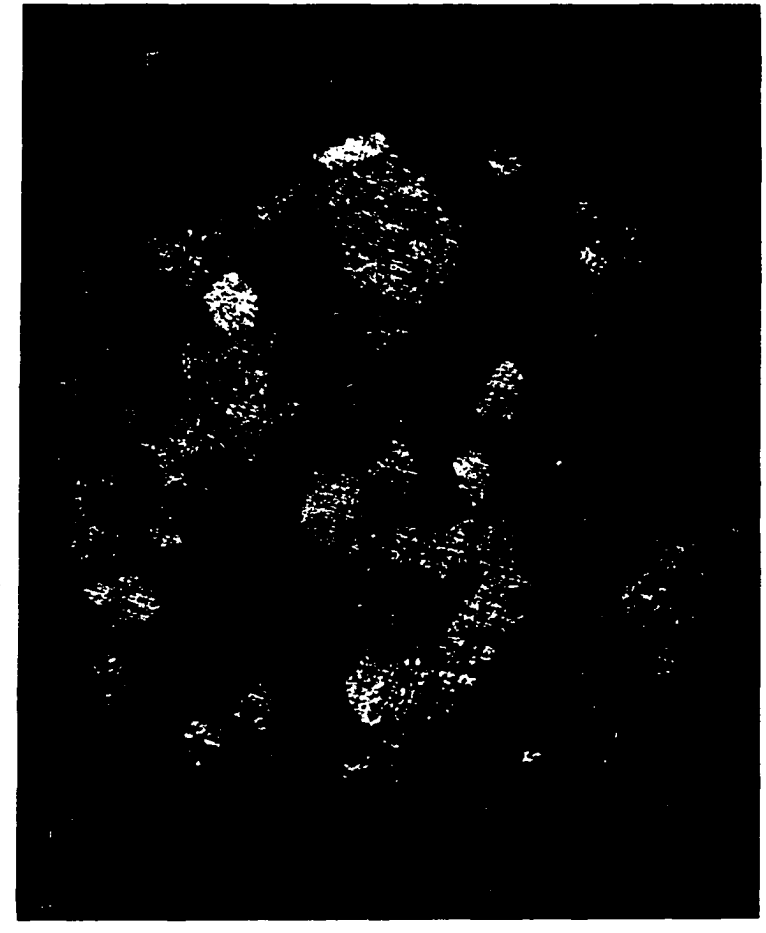

FIGURE 4.16 1/2 HR. ANNEAL

x 50 METALLOGRAPHS OF 3% In-Sn

FIGURE 4.17 1 HR. ANNEAL

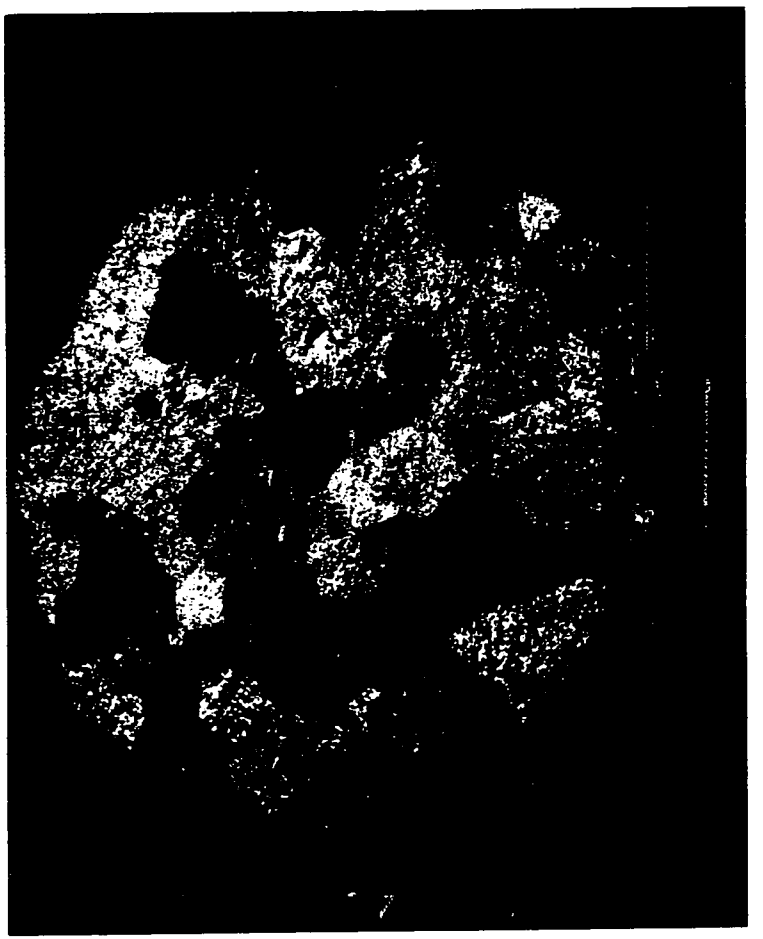

FIGURE 4.18 4 HR. ANNEAL

x 50 METALLOGRAPHS OF 3% In-Sn

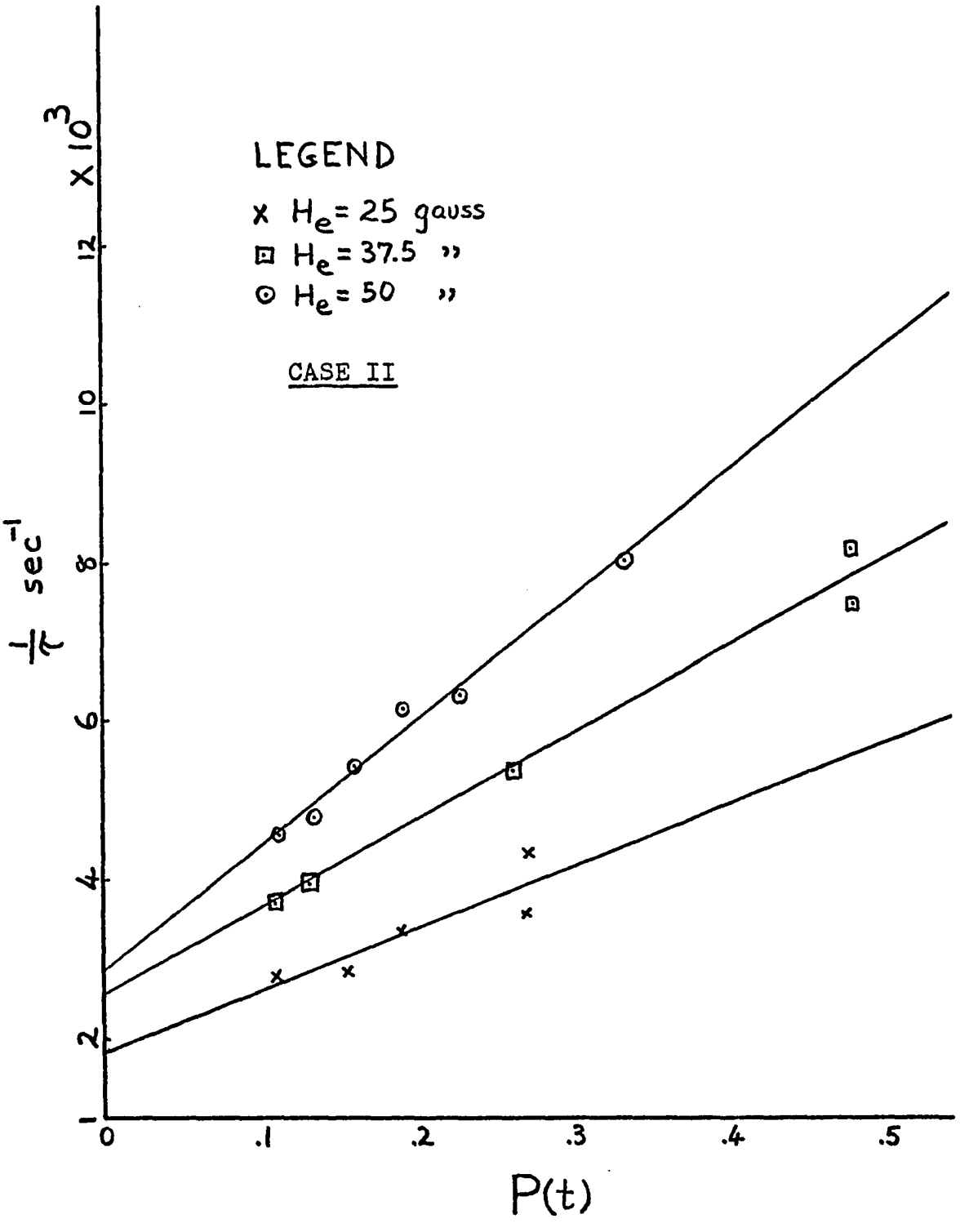

Figure 4.19 $1/\tau$ versus P(t) for 3% In-Sn, 0 hr annealing

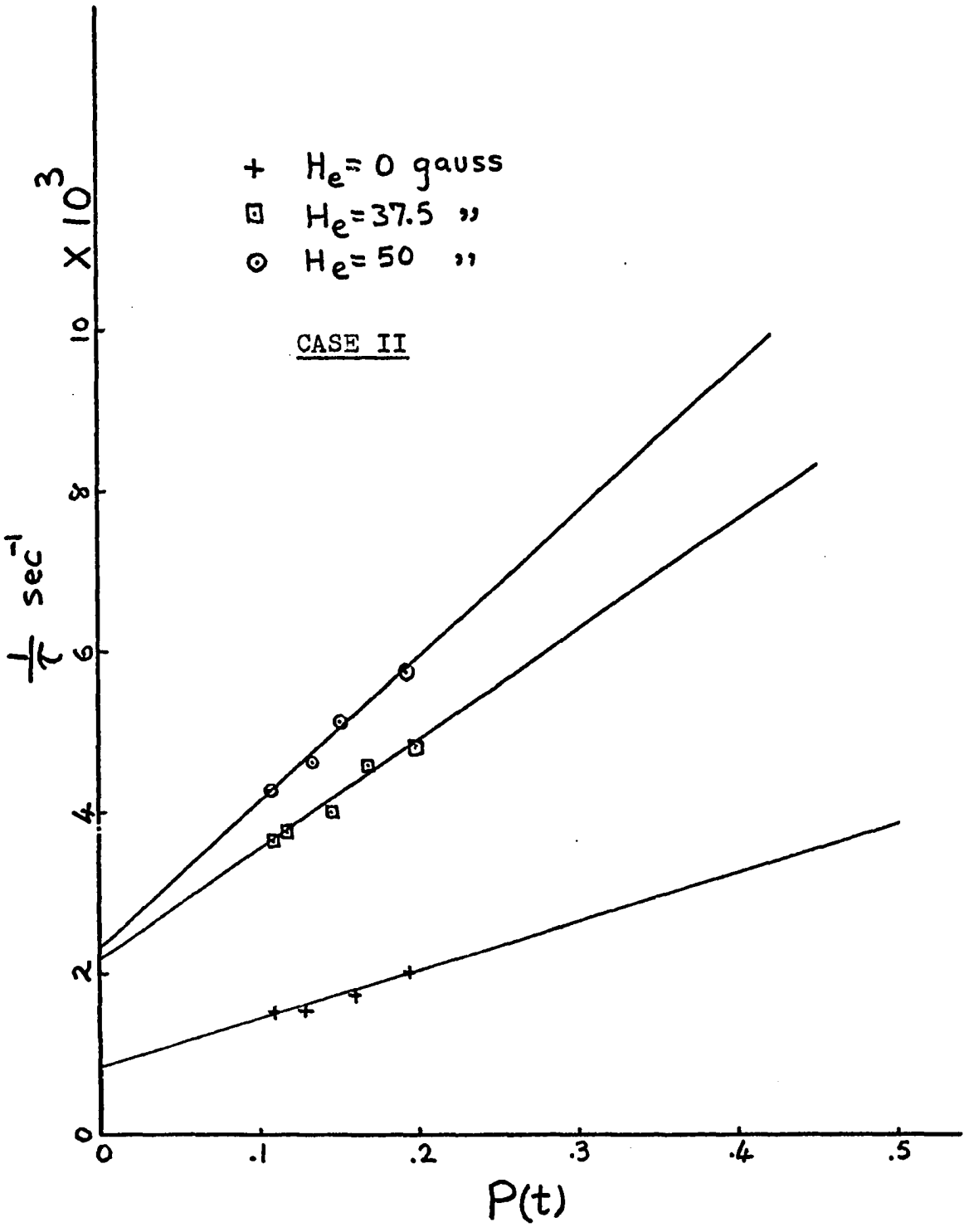

Figure 4.20 $1/\tau$ versus P(t) for 3% In-Sn, ½ hr annealing

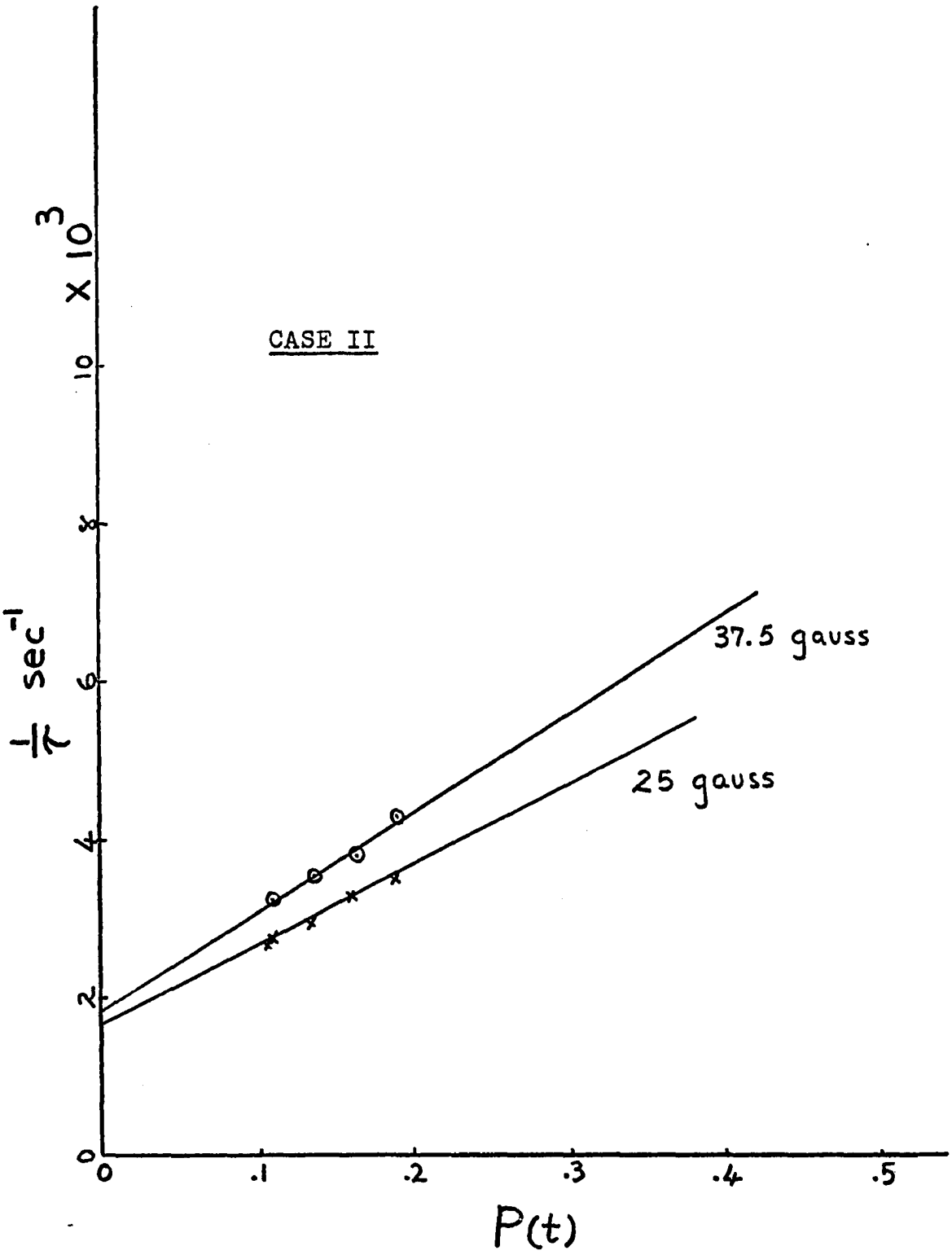

Figure 4.21 $1/\tau$ versus P(t) for 3% In-Sn, 1 hr annealing

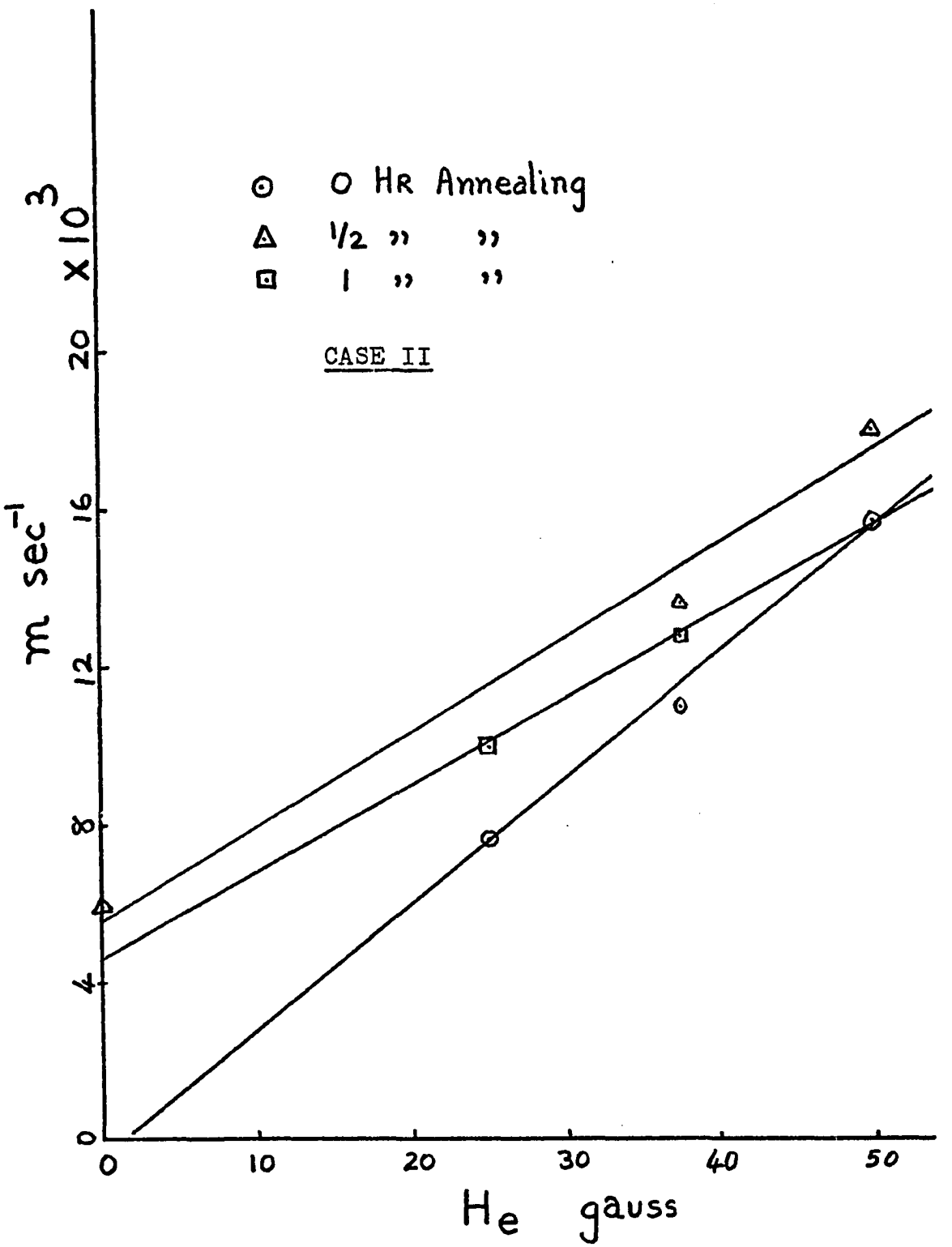

Figure 4.22 m versus H_e for 3% In-Sn

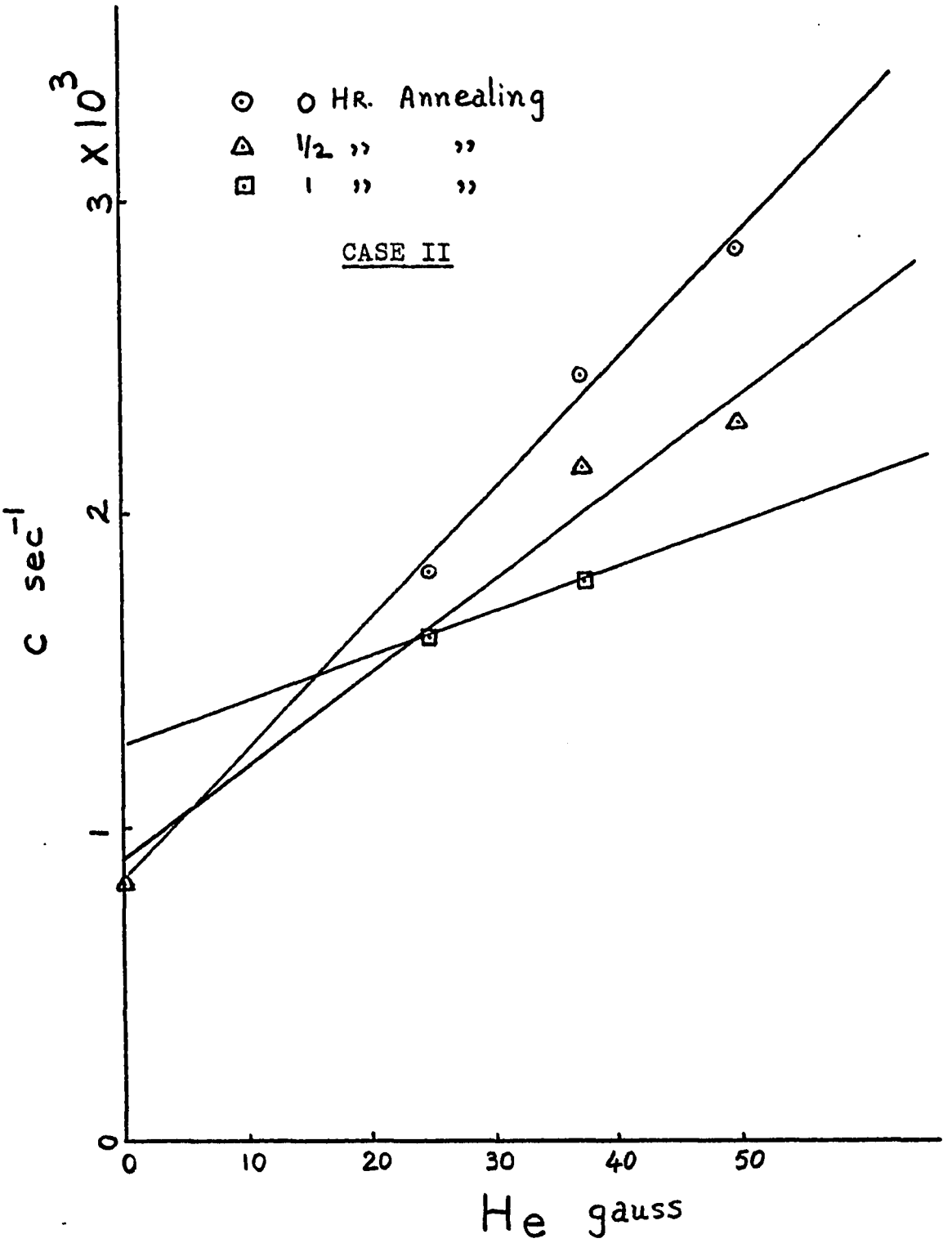

Figure 4.23 c versus H_e for 3% In-Sn

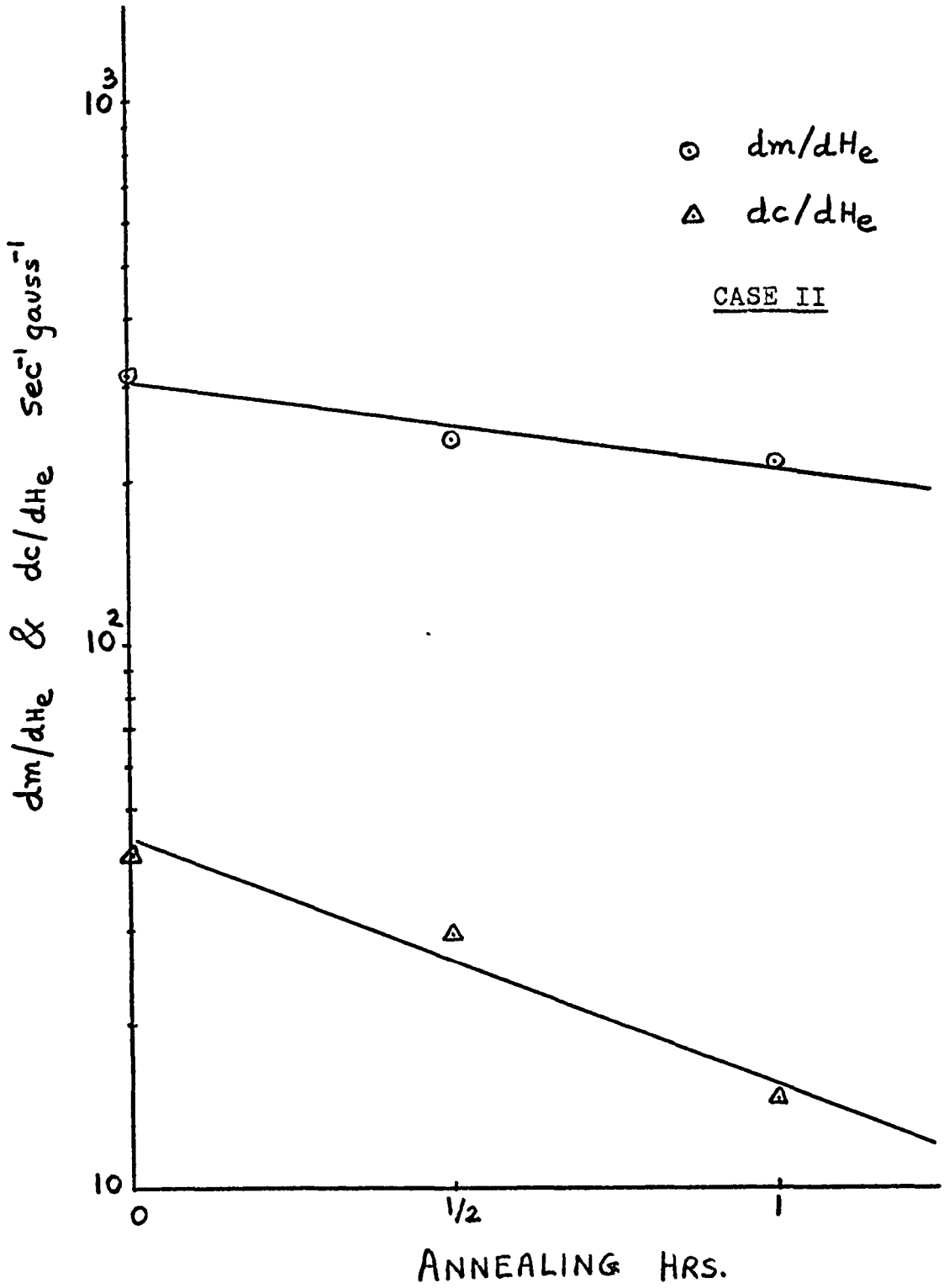

Figure 4.24 dm/dH_e and dc/dH_e versus annealing time for 3% In-Sn

the surface roughness must have increased each time the sample was cleaned after annealing. Since the surface roughness is expected to increase the losses and annealing is expected to decrease the losses, $A(\nu)$ must be a sensitive function of both the surface roughness and annealing.

Figure 4.23 is a plot of c versus H_e with annealing time as the parameter. It is found that c is a linear function of H_e. The zero-field intercepts, which are proportional to r_o in equation 4.8, are seen to be increasing with annealing and etching. This indicates that r_o must be more sensitive to surface roughness than to the state of anneal of the sample.

Finally, Figure 4.24 shows $\log(dm/dH_e)$ and $\log(dc/dH_e)$ plotted against the annealing time in hours. The plots are seen to be straight lines. Now, $dm/dH_e = k_2GA_o$ and $dc/dH_e = k_4GA_o$ where k_2, k_4 and G are all independent of the annealing time. Hence it can be inferred that for an incompletely annealed sample, A_o decays exponentially with annealing time. After a sufficiently long annealing time, A_o reduces to a value which is independent of the annealing time but which may be a function of other parameters such as impurities etc. The slopes of both the plots in Figure 4.24 should be the same. Within the limits of experimental error, this is found to be the case. From the average slope, the average time constant of the decay of A_o is found to be 1.8 hours.

From equation 2.6, since the deformity decreases exponentially with annealing time, the flux trapping sites must somehow be related to the deformities. It is probable that flux-trapping occurs at the deformities.

Summary of Results and Conclusions

The microwave method of studying flux-trapping at 12 GHz is found to be successful. Following are the findings of the research.

(1) At 12 GHz, the surface resistance of lead follows Pippard as well as AGK temperature dependence. The maximum measured Q of the lead plated cavity used in this research was 196.5×10^6 at $2.16^\circ K$.

(2) For a 3 mil thick 5% In-Sn sample annealed for 24 hours at $200^\circ C$, the fraction of area that traps flux at the transition is estimated to be 0.1; H_o is 7080 gauss and the area per fluxoid at $0^\circ K$ is 2.825×10^{-15} m^2.

(3) Flux-trapping in 3 mil thick foils of 5% and 4% In-Sn annealed for 24 hours at $200^\circ C$ is more sensitive to the state of anneal rather than the percentage of indium.

(4) Because of its low recrystallization temperature, the γ-phase tin-indium is not suitable for studying flux-trapping as a function of impurity unless it is annealed for a prolonged period of time.

(5) For a 3% In-Sn sample made in the laboratory, the area of low critical magnetic field is found to decrease exponen-

tially with the annealing time for an unannealed sample. The area of low critical magnetic field is therefore governed by the inhomogeneities in the material such as structural defects and clusters of indium atoms.

BIBLIOGRAPHY

1. K. Mendelssohn, Proc. Roy. Soc. (London), A152, 36 (1935).

2. D. L. Decker, D. E. Mapother and R. W. Shaw, Phys. Rev., 112, 1888 (1958).

3. J. D. Livingston, Phys. Rev., 129, 1943 (1963).

4. E. A. Lynton and B. Serin, Phys. Rev., 112, 70 (1958).

5. J. I. Budnick, E. A. Lynton and B. Serin, Phys. Rev., 103, 286 (1956).

6. J. W. Stout and L. Guttman, Phys. Rev., 88, 703 (1952).

7. A. B. Pippard, Phil. Trans. Roy. Soc., A248, 97 (1955).

8. P. R. Doidge, Phil. Trans. Roy. Soc., A248, 553 (1956).

9. M. Desirant and D. Shoenberg, Proc. Roy. Soc., A194, 63 (1948).

10. W. J. deHass, A. D. Engelkes and O. A. Guinau, Physica, 4, 595 (1937).

11. K. Mendelssohn, and R. B. Pontius, Nature (London), 138, 29 (1936).

12. H. London, Proc. Roy. Soc. (London) A176, 522 (1940).

13. J. Bardeen, L. N. Cooper and J. R. Schrieffer, Phys. Rev., 108, 1175 (1957).

14. D. C. Mattis and J. Bardeen, Phys. Rev., 111, 412 (1958).

15. P. B. Miller, Phys. Rev., 118, 928 (1960).

16. J. M. Pierce, H. A. Schwettman, W. M. Fairbank and P. B. Wilson, Program and Abstracts of the 9th International Conference on Low Temperature Physics, Ohio State University, August 31-September 4, 1964, p. 16.

17. J. L. Gittleman and B. Rosenblum, Proc. IEEE, 52, 1138 (1964).

18. W. M. Fairbank, Phys. Rev., 76, 1106 (1949).

19. E. Maxwell, P. M. Marcus and J. C. Slater, Phys. Rev., 76, 1332 (1949).

20. C. Roland Haden, "Flux Trapping Model for RF Losses in Superconductors", Ph. D. Dissertation, The University of Texas, August 1965.

21. J. M. Victor, "Residual Superconducting RF Losses", Ph. D. Dissertation, The University of Texas, December 1966.

22. A. B. Pippard, Nature, 162, 68 (1948).

23. J. L. Zar, J. Appl. Phys., 35, 1610 (1964).

24. J. E. Kunzler, J. Appl. Phys., 33, 1042 (1962).

25. T. P. Sheahen, Phys. Rev., 149, 368 (1966).

26. J. Halbritter, Report 3/67-2, Gesellschaft fur Kernforschung, Karlsruhe, 1967.

27. H. A. Schwettman, J. P. Turneaure, W. M. Fairbank, T. I. Smith, M. S. McAshan, P. B. Wilson and E. E. Chambers, IEEE Trans. Nucl. Sci. NS-14, No. 3, 336 (1967).

28. E. Maxwell, Prog. Cryogenics, 4, 125 (1964).

29. A. A. Abrikosov, L. P. Gor'kov and I. M. Khalatnikov, Soviet Physics J. E. T. P. 8, 182 (1959); 10, 132, (1960).

30. J. E. Kunzler, Materials Research and Standards, April 1965, pp 161-171.

31. H. Hahn, H. J. Halama and E. H. Foster, J. Appl. Phys., 39, 2606 (1968).

32. I. G. Wilson, C. W. Schramm and J. P. Kinzer, Bell System Tech. J., 25, 408 (1946).

33. C. W. Richards, Engineering Materials Science, Wadsworth Publishing Co., San Fransisco, 1961, p. 256.

34. B. Chalmers, Physical Metallurgy, John Wiley and Sons, New York, 1962, p. 305 and p. 249.

35. E. A. Lynton, Superconductivity, Methuen and Co., London 1969.

36. R. E. Collin, Foundations for Microwave Engineering, McGraw Hill Book Co., 1966, p. 327.

37. Ramo, Whinnery and Van Duzer, Fields and Waves in Communication Electronics, John Wiley and Sons, New York, 1965.

APPENDIX

EXPERIMENTAL DATA

Data on Lead with $H_e < 3$ mG

Run #	T(°K)	τ μsec	Q_o x10^6	P(t)	r_{exp}	r_{AGK}
1	4.16	380	14.32	0.09455	0.0097703	0.001210
	3.65	650	24.5	0.05656	0.005264	0.000673
2	3.2	1152	43.4	0.034	0.002971	0.000369
	3.0	1390	52.3			
	2.692	2485	93.65			
	2.2	1785	67.2			
	2.06	1184	44.7			
5	3.013	1417.5	53.4	0.027	0.002415	0.000279
	2.42	3175	119.7	0.01167	0.001077	0.0000918
	2.16	5215	196.5	0.007532	0.000656	0.0000468

Data on 5% In-Sn Annealed for 24 Hours at 200°C

$T_c = 3.64°K$

Run #	Magnetic Field Gauss	T(°K)	τ μsec	$1/\tau$ sec^{-1}	P(t)
3	< 0.003	3.187	146.9	6807.3	0.8067
		2.916	272.8	3665.7	0.4265
		2.6	455.0	2197.8	0.233
		2.28	727.5	1374.5	0.1306
		2.2	798.0	1253.1	0.1128
	4.0	3.196	82.9	12062.7	0.8272
		2.7	175.7	5691.5	0.28
		2.395	310.0	3225.8	0.161
		2.2	338.1	2957.7	0.1128
	9.9	3.2	52.3	19120.0	0.8366
		2.7	117.9	8481.7	0.28
		2.31	167.1	5984.4	0.138
		2.2	170.5	5865.1	o.1128

Data on 5% In-Sn Sample Annealed for 24 Hours at 200°C

$T_c = 3.64°K$

Run #	Magnetic Field Gauss	T(°K)	τ μsec	$1/\tau$ sec^{-1}	P(t)
4	< 0.003	3.0	245.8	4068.34	0.51
	6.5	3.2	127.4	7849.3	0.8366
		3.0	180.5	5540.1	0.510
		2.8	250.8	3987.2	0.3385
		2.5	438.0	2283.1	0.1945
		2.34	546.5	1829.8	0.1457
		2.2	761.0	1314.06	0.1128
	20.0	3.2	95.5	10471.2	0.8366
		2.79	193.3	5173.3	0.3320
		2.495	300.0	3333.3	0.1927
		2.13	404.5	2472.2	0.0989
	40.0	3.2	74.7	13386.8	0.8366
		2.99	104.7	9551.1	0.499
		2.794	137.8	7256.9	0.3346
		2.5	177.7	5627.5	0.1945
		2.2	245.5	4073.3	0.1128
		2.2	251.5	3976.14	0.1128
	70.0	2.8	92.8	10775.8	0.3385
		2.6	125.0	8000.0	0.233
		2.4	147.2	6793.47	0.1624
		2.2	163.7	6108.7	0.1128
		2.18	154.8	6459.95	0.1087

Data on 4% In-Sn Sample Annealed for 24 Hours at 200°C

$T_c = 3.645°K$

Run #	Magnetic Field Gauss	T(°K)	τ μsec	$1/\tau$ sec^{-1}	P(t)
6	< 0.003	3.0	250.7	3988.80	0.5055
		2.7	276.7	3614.00	0.2780
		2.6	314.3	3181.60	0.2315
		2.5	337.0	2967.30	0.1933
		2.4	356.0	2808.90	0.1610
		2.3	364.8	2741.20	0.1347
		2.2	366.8	2969.10	0.1120
		2.2	380.0	2631.50	0.1120
	25.0	3.006	101.5	9852.2	0.5123
		2.8	139.0	7194.2	0.3360
		2.6	176.25	5673.7	0.2315
		2.4	203.5	4914.0	0.1610
		2.195	252.0	3968.2	0.1111
	50.0	3.0	71.2	14045.0	0.5055
		2.8	97.5	10256.0	0.3360
		2.7	107.0	9345.8	0.2780
		2.6	113.5	8810.6	0.2315
		2.5	122.5	8163.2	0.1933
		2.4	127.0	7874.0	0.1610
		2.3	142.5	7017.5	0.1347
		2.2	150.0	6666.7	0.1120
	75.0	3.0	40.4	24752.4	0.5055
		2.8	42.6	23474.0	0.3360
		2.7	58.0	17241.0	0.2780
		2.6	63.0	15873.0	0.2315
		2.48	75.2	13297.8	0.1861
		2.4	80.8	12376.2	0.1610
		2.3	77.2	12953.3	0.1347
		2.2	84.8	11792.4	0.1120

Data on 13% In-Sn Sample Annealed for 29.5 Hours at 173°C

Run #	Magnetic Field Gauss	T(°K)	τ μsec
7	< 0.003	4.2	20.0
		3.0	178.0
		2.8	237.0
		2.6	253.0
		2.49	260.0
		2.395	291.5
		2.3	287.5
		2.2	288.0
	50.0	2.8	195.0
		2.6	219.0
		2.486	192.0
		2.387	203.0
		2.3	233.0
		2.2	239.0
	75.0	2.8	167.0
		2.6	188.0
		2.49	196.0
		2.4	197.0
		2.3	196.0
		2.2	197.0
		2.2	205.0
8	0.003	3.0	243.0
		2.79	285.0
		2.6	277.0
		2.5	212.0
		2.4	310.0
		2.3	373.5
		2.2	347.0
		2.2	347.5
9	0.003	2.585	281.0
		2.473	283.0
		2.387	300.0
		2.387	333.0
		2.387	327.5
		2.273	327.5

	2.273	332.0
	2.27	324.0
	2.27	332.0
	2.184	345.0
	2.177	345.0
25.0	2.894	287.5
	2.795	399.0
	2.775	317.0
	2.68	342.0
	2.68	320.0
	2.68	315.0
	2.582	339.0
	2.503	325.0
	2.36	347.0
	2.36	370.0
	2.23	350.0
	2.195	368.0
50.0	2.964	251.0
	2.833	303.0
	2.711	300.0
	2.52	286.0
	2.52	328.0
	2.35	350.0
	2.185	356.0
75.0	2.86	182.5
	2.745	204.0
	2.57	205.0
	2.413	205.0
	2.27	220.0
	2.2	211.5
	2.2	225.0
100.0	2.884	93.0
	2.56	109.0
	2.4	108.0
	2.26	133.0

Data on As-rolled 3% In-Sn Sample

$T_c = 3.65^{\circ}K$

Run #	Magnetic Field Gauss	T($^{\circ}$K)	τ μsec	$1/\tau$ sec^{-1}	P(t)
10	25.0	2.69	230.0	4347.83	0.2711
		2.688	280.0	3571.43	0.2701
		2.49	300.0	3333.33	0.1886
		2.38	352.0	2840.91	0.1548
		2.285	352.0	2840.91	0.1303
		2.19	357.0	2801.12	0.1090
	37.5	2.98	122.0	8196.70	0.4798
		2.98	134.0	7462.69	0.4798
		2.67	185.0	5405.40	0.2610
		2.29	249.0	4016.06	0.1310
		2.29	252.0	3968.25	0.1310
		2.185	266.0	3759.40	0.1084
		2.185	269.0	3717.47	0.1084
	50.0	2.8	124.0	8064.52	0.3335
		2.598	158.0	6329.11	0.2290
		2.5	162.0	6171.29	0.1921
		2.4	184.0	5434.78	0.1605
		2.3	209.0	4784.69	0.1340
		2.2	218.0	4587.15	0.1115

Data on 3% In-Sn Sample Annealed for ½ Hour at 200°C

$T_c = 3.65°K$

Run #	Magnetic Field Gauss	T(°K)	τ μsec	$1/\tau$ sec^{-1}	P(t)
11	< 0.003	2.505	494.0	2024.29	0.1938
		2.393	575.0	1739.13	0.1580
		2.393	575.0	1739.13	0.1580
		2.281	656.0	1524.39	0.1290
		2.198	665.0	1503.76	0.1111
		2.198	648.0	1543.21	0.1111
	37.5	2.522	207.0	4830.92	0.1990
		2.431	218.0	4587.148	0.1690
		2.35	250.0	4000.00	0.1466
		2.227	267.0	3745.32	0.1172
		2.196	272.0	3676.47	0.1100
		2.195	273.0	3663.00	0.1100
	50.0	2.5	174.0	5747.13	0.1921
		2.5	174.0	5747.13	0.1921
		2.37	195.0	5128.20	0.1520
		2.305	217.0	4608.29	0.1350
		2.19	233.0	4291.85	0.1090

Data on 3% In-Sn Sample Annealed for 1 Hour at 200°C.

$T_c = 3.65°K$

Run #	Magnetic Field Gauss	T(°K)	τ μsec	$1/\tau$ sec^{-1}	P(t)
12	25.0	2.49	286.0	3496.50	0.1886
		2.398	304.0	3289.47	0.1600
		2.30	343.0	2915.45	0.1340
		2.195	364.0	2747.25	0.1100
		2.175	373.0	2680.96	0.1060
	37.5	2.494	233.0	4291.85	0.1900
		2.408	265.0	3773.58	0.1630
		2.304	285.0	3508.77	0.1350
		2.19	310.0	3225.81	0.1090